6.0 Predictive studies of helium beam attenuation and emission

6.1 Introduction

During tokamak experiments it is convenient to keep the neutron flux from the plasma to a minimum so that access to the vessel may be unrestricted. To minimise the beam driven neutron production rate, fast helium beam atoms can be injected into the plasma instead of neutral deuterium atoms. The neutral helium beams still heat the fusion plasma but without the production of unwanted neutrons[84]. There are also potential diagnostic benefits of injecting neutral helium beam atoms into the plasma rather than deuterium atoms. Due to the efficiency of the resonant process of double charge exchange, helium beam atoms in their ground state can act as donors to the fully stripped alpha particles contained in the plasma. The neutralised alpha particles can be measured and the associated slowing down time can be obtained[22]. Also due to the presence of metastable levels in the beam, preferential charge exchange between the ground state and the He(2 ^{3}S) metastable may be possible. As suggested by Hoekstra[85], in circumstances where the He(2 ^{3}S) metastable population is significant it may be the case that it will be primary donor for the CVI(n=8 -7) charge exchange line, with a small contribution from the He(1 ^{1}S) ground state. Where as the He(1 ^{1}S) ground state would be the primary donor for the HeII(n=4-3) charge exchange line, with a small contribution from the He(2 ^{3}S) metastable. Another important diagnostic benefit is with the application of beam emission spectroscopy. Due to the degenerate nature of deuterium atoms, the motional Stark effect resulted in a complicated array of Stark components which was difficult to analyse (see chapter 5.0). In the case of neutral helium, the influence of the motional Stark effect on the observed emission lines is not as significant and so the spectrum is simpler to analyse.

In this chapter we show the behaviour and parameter dependencies of the helium beam collisional-radiative ionisation and cross coupling coefficients required to model the beam attenuation and the non-equilibrium metastable populations. In particularly, we highlight the difference in the rate at which electrons are ionised from the ground state and the two metastables. We also explore the parameter dependencies of the quasi-static excited population structure required to predict the

emission from the beam atoms themselves and hence extract the local plasma conditions from measurements. We examine in detail the influence of the non-equilibrium metastables on the quasi-static excited populations of the levels contained in the n=4 shell. The motivation for this is that if we can identify which metastable is most effective at populating each of the levels in the n=4 shell, we can utilise the spectral emission originating from the n=4 shell of the beam atoms to gauge the metastable content of the beam.

Focusing our attention on the metastability associated with the He(2 ^{1}S) and He(2 ^{3}S) levels, we investigate the implications of assuming that the metastables have relaxed and reached equilibrium relative to the ground state. To achieve this we calculate the metastable populations, for JET plasma conditions, using a spatial dependent treatment and we compare the results with that obtained from the quasi-static approximation.

Finally, we consider the attenuation of the neutral helium beam. We investigate the attenuation of ground state and metastable populations and study the influence of changing the initial metastable fractions of the beam. We also briefly consider the influence of sudden changes in the electron temperature and density. Our main motivation here is to describe quantitatively what happens to the metastable populations as the beam progresses through the plasma.

6.2 Review of the collisional-radiative coupling coefficients

It was discussed at length in chapter 2.0 the origin and application of the collisional-radiative cross coupling coefficients. It is worth briefly reviewing the main features at this point. To calculate the beam attenuation and the non-equilibrium level populations we construct a set of coupled equations using the collisional-radiative cross coupling coefficients. As mentioned earlier the coupling coefficients take into consideration the influence of stepwise atomic processes. For example the cross coupling coefficient which describes the rate at which the He(2 ^{3}S) metastable is populated by the He(1 ^{1}S) ground state will include the influence of all possible reaction pathways rather than just the rate for direct excitation. The coupled equations are of the form,

$$
\begin{aligned}
v_b \frac{dN_{1^1S}}{dx} &= n_e S_{1^1S} N_{1^1S} - n_e S_{2^1S \to 1^1S} N_{2^1S} - n_e S_{2^3S \to 1^1S} N_{2^3S} \\
v_b \frac{dN_{2^1S}}{dx} &= -n_e S_{1^1S \to 2^1S} N_{1^1S} + n_e S_{2^1S} N_{2^1S} - n_e S_{2^3S \to 2^1S} N_{2^3S} \\
v_b \frac{dN_{2^3S}}{dx} &= -n_e S_{1^1S \to 2^3S} N_{1^1S} - n_e S_{2^1S \to 2^3S} N_{2^1S} + n_e S_{2^3S} N_{2^3S}
\end{aligned}
\qquad 6.1
$$

where v_b and n_e are respectively the beam velocity and the electron density. The quantity dx is along the beam path and $N_{n\,^{2S+1}L}$ represents the population of the non-equilibrium level specified by the quantum numbers n, L and S. The collisional-radiative cross coupling coefficients are represented by the symbol $S_{n^{2S+1}L \to n^{2S+1}L}$, where the subscripts specify the initial and final non-equilibrium level. The cross coupling coefficients for which the subscript only specifies the initial state e.g. $S_{n^{2S+1}L}$, refer to what can be described as the total loss coefficient from the level $n^{2S+1}L$. The total loss coefficient includes the collisional-radiative ionisation rate from the level $n^{2S+1}L$ as well as the contribution to populating the remaining levels. As discussed in chapter 2.0, the collisional-radiative ionisation coefficients represent the rate at which the non-equilibrium levels of the beam atoms are ionised and are obtained from the cross coupling coefficients using the following expression,

$$
S_\rho = S_{\rho\rho} - \sum_{\sigma=1}^{\rho-1} S_{\rho\sigma} - \sum_{\sigma=\rho+1}^{m} S_{\rho\sigma} \qquad 6.2
$$

where S_ρ and $S_{\rho\sigma}$ are respectively the effective ionisation and cross coupling coefficients, and the subscripts ρ and σ represent the initial and final states. In figure 6.1 we schematically show the physical significance of the collisional-radiative ionisation and cross coupling coefficients.

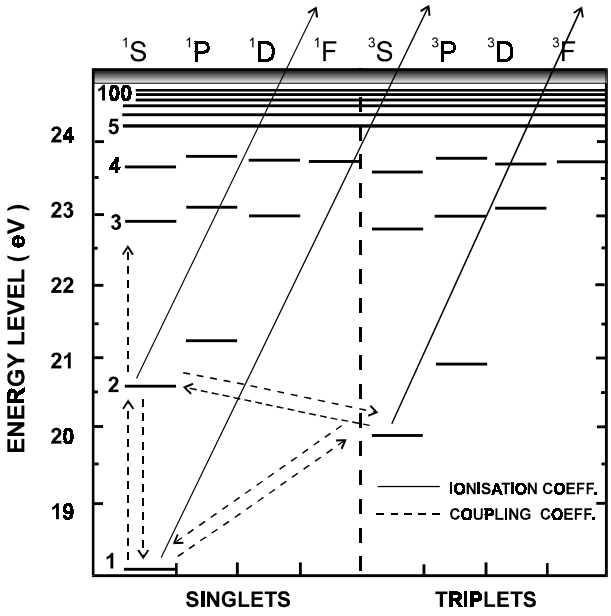

Figure 6.1 Schematic illustration of the energy levels structure of neutral helium. Highlighted with the dashed lines are the collisional-radiative cross coupling coefficients. Also shown in the figure with the solid lines are the effective ionisation coefficients associated with each metastable level. Note that the coefficients which connect two metastables include the influence of all indirect paths.

6.3 Collisional-radiative cross coupling coefficients

The cross coupling coefficients describe the rate at which the metastable levels, including the ground state, are populated and depopulated within a collisional-radiative frame work. They include the influence of stepwise atomic processes and can be used to define an effective ionisation coefficient associated with the ground state and each metastable. In figure 6.2 we show the behaviour of the cross coupling and effective ionisation coefficients as a function of beam energy for a pure D^+ plasma.

The parameter dependencies which are of interest are the electron density, neutral beam energy and the electron temperature. We also wish to separate the contributions to the coupling coefficients due to electron and ion collisions and finally, explore the dependence on the nuclear charge of the impurity ions contained in the plasma. We have categorised the coupling coefficients into two groups of similar parameter dependency. The first group are associated with spin changing transitions, while the second group contains the remaining coefficients and is referred

to as the non-spin changing group. It should be noted that in the present work all of the coefficients are calculated in terms of the electron density with the condition of charge neutrality imposed.

Figure 6.2 Collisional-radiative cross coupling and effective ionisation coefficients for a pure D^+ plasma. Working down from the top we first consider the coefficients associated with the He($1\ ^1S$) ground state and then the He($2\ ^1S$) and He($2\ ^3S$) metastables. Also shown are the effective ionisation coefficients. The electron density was 1.0×10^{13} cm^{-3} and the electron temperature was 100 eV.

6.3.1 Non spin changing transitions

The cross coupling coefficients which have been categorised into the non-spin changing group are schematically shown in figure 6.3.

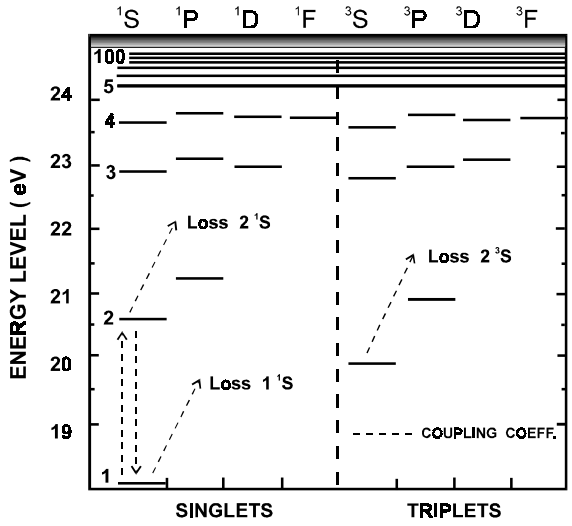

Figure 6.3 Schematic illustration of the five effective coupling coefficients which have been placed in the non-spin changing category.

There are five coupling coefficients in the non-spin changing group. The coefficients which connect the He(1 ^{1}S) and the He(2 ^{1}S) levels are the true cross coupling coefficients while the remaining three coefficients describe the total rate at which electrons are lost from each level. The latter contain the effective ionisation coefficient, as well as the coupling coefficients which connect to the other two remaining levels. We use the name 'cross coupling' coefficient to refer to all these types of effective coefficients

We shall first consider the density dependence of a non spin changing coupling coefficient for a pure D^+ plasma. In figure 6.4 we illustrate the behaviour of the coupling coefficient, which describes the total loss rate associated with the He(1 ^{1}S) ground state, as a function of beam energy for three different densities. The electron densities which have been selected to represent the coronal, collisional-radiative and high density regimes are 10^6, 10^{13} and 10^{15} cm^{-3} respectively.

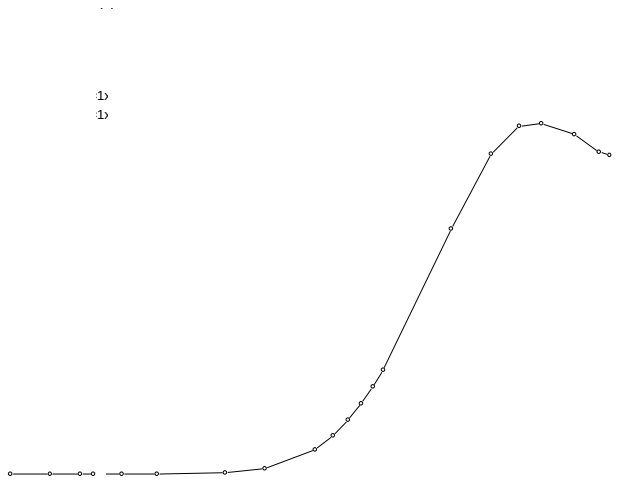

Figure 6.4 Cross coupling coefficient describing the total loss rate from the He(1 ^{1}S) ground state for a pure D^+ plasma . The coefficient has been plotted for three different densities as a function of neutral beam energy. Also shown in the figure is the contribution to the coefficient due to electrons collisions only. The electron temperature was 100 eV.

In the coronal regime only the direct processes contribute to the coefficient. The component of the cross coupling coefficient which represents the effective ionisation coefficient is just the rate for direct ionisation due to electrons and ions, while the remaining component of the cross coupling coefficient, which connects the He(1 ^{1}S) ground state to the other two metastables levels, is simply the sum of the corresponding direct excitation rates. When the electron density is increased to around 1 x 10^{13} cm^{-3} , we are in the collisional-radiative regime where the role of stepwise atomic processes is important. This results in an overall increase in the effective cross coupling coefficient. The effective ionisation component of the coupling coefficient now includes a contribution due to ion and electron impact ionisation from excited levels and the remaining component of the coupling coefficient includes the influence of stepwise atomic processes. At an electron density of 1.0 x 10^{15} cm^{-3}, we are in the high density regime, see figure 6.4. The coupling coefficient has reached a maximum value. The component of the coupling coefficient which represents the effective ionisation rate includes the influence of ion

and electron impact ionisation from the ground and the excited states. Even excitation contributes to ionisation. The contribution of the cross coupling coefficient which connects the ground state with the two metastable levels now includes the full influence of stepwise processes as well as direct excitation.

It is of interest to contrast the behaviour of the cross coupling coefficient calculated with and without the inclusion of ions. As can be observed in figure 6.4, the contribution to the effective coefficient due to electrons, regardless of the electron density, is independent of the beam energy. This is due to the fact that the electrons are moving in the plasma with such a large velocity that the speed of the beam is insignificant. If however we introduce ions into the plasma the effective coefficient changes. In the low energy regime the contribution to the cross coupling coefficient is primarily due to electrons. The ions collisions are only driven by their thermal ion temperature and the net contribution is small. As the neutral beam energy is increased the influence of the ion collision becomes significant and results in an increase in the effective coupling coefficient, see figure 6.4. The increase in the coupling coefficient directly reflects the energy dependence of the cross sections which describe the behaviour of ion impact excitation and ionisation The latter being of greater importance above 10 keV amu^{-1}.

The temperature dependence of the coupling coefficient is the next issue we want to address. In figure 6.5 we show for a low density D^+ plasma ($\sim 1.0 \times 10^6$ cm^{-3}), the coupling coefficient which described the total loss rate associated with the He($1\,^1S$) ground state as a function of the beam energy for a selected range of temperatures.

It can be observed that an increase in the electron temperature results in an increase in the coupling coefficient. This is due to the temperature dependence of the electron collisions which contribute to the cross coupling coefficient. At a temperature of 10 eV the component of the coupling coefficient which represents the effective ionisation coefficient is simply the corresponding electron impact ionisation rate. As we increase the temperature, the behaviour of the effective ionisation component reflects the behaviour of electron impact ionisation rate. It is of interest to note that as we increase the temperature from 10 to 100 eV there is a substantial

increase in the coupling coefficient. However as we increase the temperature from 100 to 1 keV the change in the coupling coefficient is less. This is a clear illustration of the temperature dependence of the electron collisions, particularly the electron impact ionisation rate which is also shown in figure 6.5. We also show in figure 6.5 the contribution to the coupling coefficient due to electron collisions alone. As before we can observe that the electron contribution is independent of the beam energy and is governed by the electron temperature.

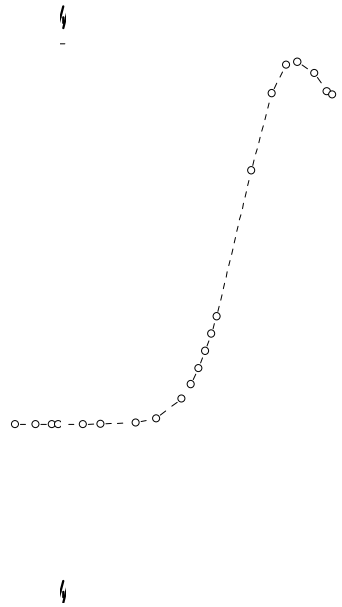

Figure 6.5 Temperature dependence of the coupling coefficient describing the total loss rate associated with the He(1 ^{1}S) ground state for a pure D^+ plasma. The plot on the left illustrate the coupling coefficient as a function of neutral beam energy for a selected range of electron temperatures. Also shown is the contribution to the coupling coefficient due to electron collisions. The electron density was 1.0 x 10^6 cm^{-3} .The plot on the right illustrates the temperature dependence of the electron impact ionisation rate coefficient associated with the He(1 ^{1}S) ground state.

Due to the unavoidable presence of impurities in tokamak plasmas we must also take into consideration their influence on the cross coupling coefficients. In figure 6.6 we show the behaviour of the coupling coefficient which describes the total loss rate associated with He(1 ^{1}S) ground state for pure impurity plasmas. The electron density is fixed and the number density for each impurity species is such that charge

neutrality is maintained. Therefore as the nuclear charge of the impurity species increases the corresponding impurity number density decreases.

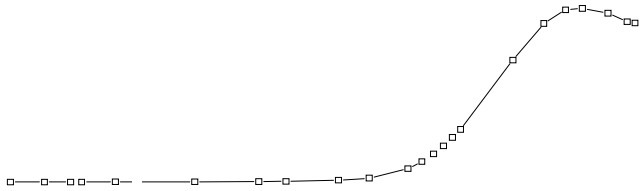

Figure 6.6 Cross coupling coefficient associated with the He(1 ^{1}S) ground state as a function of neutral beam energy for a range of pure impurity plasmas. The electron density is fixed at 1.0×10^{13} cm^{-3} and the number density of impurity species is such that charge neutrality is maintained. The electron temperature was 100 eV.

In the low energy regime the contribution to the coupling coefficient is primarily dominated by electron collisions. It can be observed however that some of the impurity ions are capable of effectively contributing to the coupling coefficient at such a low energy. Their influence in this case is due to their thermal ion temperature. As the beam energy is increased, the influence of ion impact excitation becomes important at around 10^4 eV/amu and as the beam energy is increased further ion impact ionisation dominates. The influence of the impurity ions as shown in figure 6.6, increases with nuclear charge, even though the number density of the impurity species decreases.

As mentioned before, all of the coefficients grouped into the non-spin changing category exhibit a similar type of parameter dependency and we have focused on the coupling coefficient associated with the He(1 ^{1}S) ground state merely

as an example. In figure 6.7 we show the behaviour of the coupling coefficient which describes the total loss rate associated with the He(2 ^{3}S) metastable for a pure D^+ plasma.

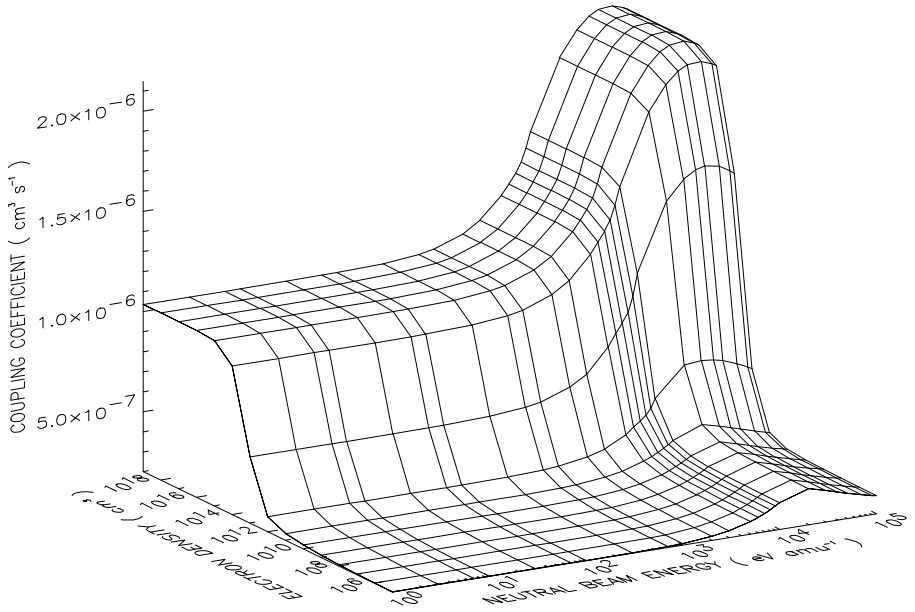

Figure 6.7 Behaviour of the cross coupling coefficient describing the total loss rate associated with the He(2 ^{3}S) metastable for a pure D^+ plasma. In the low energy regime the contribution to the coefficient is primarily driven by electron collisions. As the beam energy is increased the role of ion collisions becomes significant and an increase in the coupling coefficient can be observed. If we increase the electron density the role of step wise atomic processes becomes important and results in the coupling coefficient increasing to a maximum value which corresponds to the high density limit.

As can be observed, in the low energy region the contribution to the coupling coefficient is small, it is driven purely by electrons. As we increase the beam energy the influence of the ion collisions becomes significant and results in an increase in the coupling coefficient. An increase in the electron density encourages the atomic processes associated with the excited states to contribute to the coupling coefficient. If we continue to increase the density the high density limit is reached and the coupling coefficient tends to a constant value.

6.2.2 Spin changing transitions

We schematically show in figure 6.8 the cross coupling coefficients which are contained in the spin changing group.

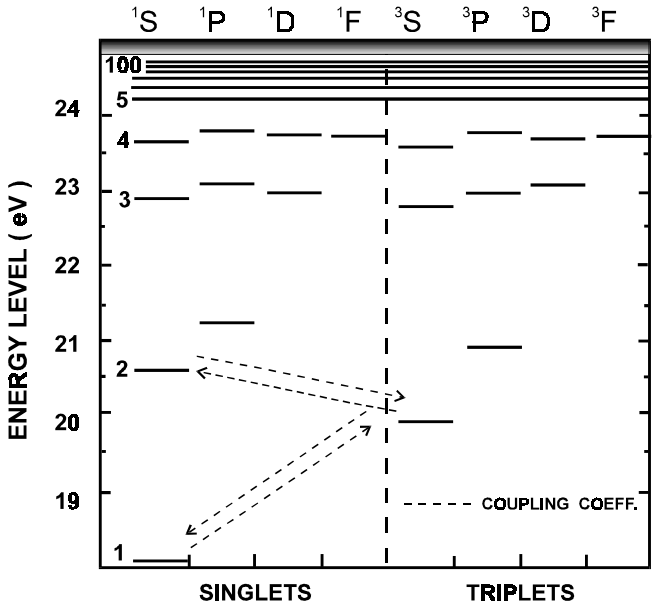

Figure 6.8 Schematic illustration of the four collisional-radiative cross coupling coefficients which are contained in the spin changing group.

There are four cross coupling coefficients in total. Each of the coefficients represent the rate at which the metastable levels, including the ground state, are populated and depopulated through spin changing processes. It is important to mention that ion collisions are strictly spin conserving. Only electron collisions are involved in spin changing transitions. Therefore in the present context the ions collisions can only populate the singlet spin systems of the beam atoms by promoting electrons from the ground state. Electron collisions however can contribute to populating both the singlet and triplet spin systems through a variety of spin and non-spin changing transitions.

We shall first consider the density dependence of the spin changing cross coupling coefficients for a pure D^+ plasma. In figure 6.9 we show the behaviour of the coupling coefficient for the transition He(2 ^{1}S)→He(2 ^{3}S) as a function of beam

energy for three different densities. Also shown are the cross coupling coefficients for a pure electron plasma.

Figure 6.9 Collisional-radiative cross coupling coefficient for the He(2 ^{1}S)→He(2 ^{3}S) spin changing transition for a pure D^+ plasma. The coupling coefficient has been plotted as a function of neutral beam energy for three different electron densities. The electron temperature was 100 eV.

As can be observed, in the above figure we are presented with some interesting results. Since electron collisions drive the spin changing transitions it would have been expected that the cross coupling coefficient would have been independent of the neutral beam energy. This is in fact the case when we look at the cross coupling coefficient as a function of beam energy in the low density regime at 1 x 10^6 cm^{-3}. However as we increase the electron density the role of atomic processes associated with excited states comes into to play. At a density of around 1 x 10^{13} cm^{-3}, as shown in figure 6.9, in the low energy regime the cross coupling coefficient is driven purely by electron collisions and is therefore independent of the beam energy. As we increase the beam energy the influence of the ion collisions becomes important. In the above figure it can be seen that the ion collisions contribute to reducing the cross coupling coefficient. This phenomena can be attributed to the fact that in the low density regime the reaction path ways from the He(2 ^{1}S) metastable is dominated by

spin changing electron collisions, even at high beam energies. As we increase the density the influence of the ion collisions contribute to increasing the reaction path ways associated with the He(2 ^{1}S) metastable level. As the beam energy increases it becomes more favourable to excite or ionise the contents of the He(2 ^{1}S) level rather than contributing to populating the He(2 ^{3}S) metastable via a spin changing transitions, see figure 6.10. The energy dependence of the spin changing cross coupling coefficients should be consider as a secondary effect .

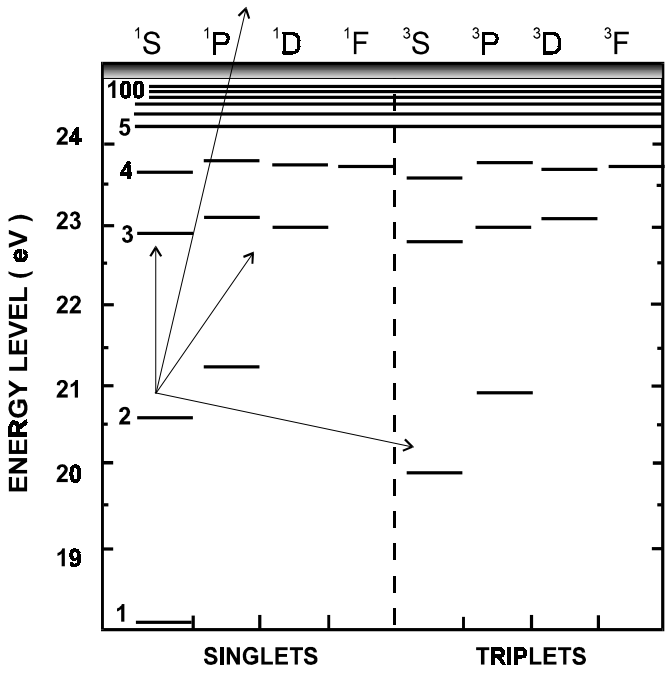

Figure 6.10 Schematic illustration of the increasing reaction pathways associated with the He(2 ^{1}S) metastable level. In the low density region the contents of the He(2 ^{1}S) metastable acts as a source to populate the He(2 ^{3}S) metastable. As the electron density is increased the role of ion collisions result in the content of the He(2 ^{1}S) metastable being preferentially excited or ionised rather than contributing to populating the He(2 ^{3}S) metastable, particularly as high energies.

We now consider the temperature dependence of the spin changing cross coupling coefficient. In figure 6.11 we show the behaviour of the cross coupling coefficient for the transition He(2 ^{3}S)$\rightarrow$ He(2 ^{1}S).

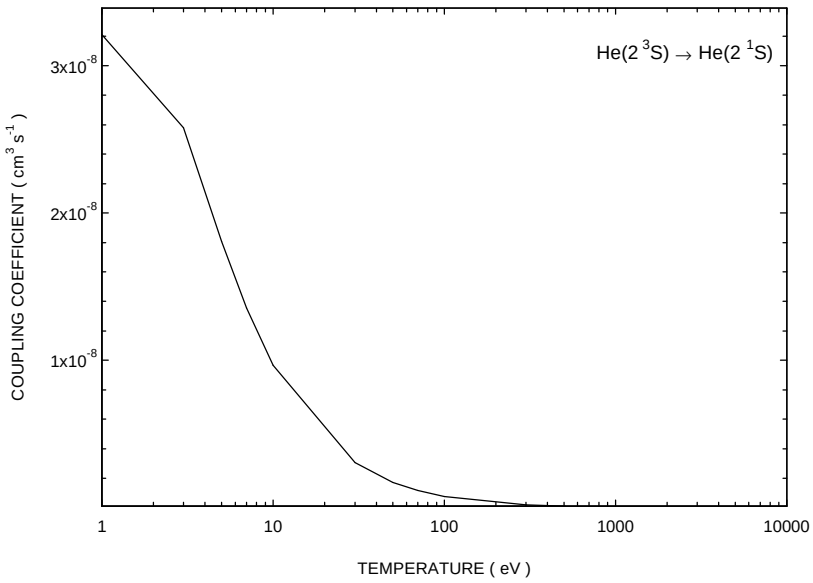

Figure 6.11 Temperature dependence of the cross coupling coefficient for the transition He(2 ^{3}S)→ He(2 ^{1}S). The behaviour of the cross coupling coefficient directly reflects the temperature dependence of the fundamental data.

Spin changing transition are driven purely by the electron collisions and since the influence of the electron collision is governed by the temperature we would expect a strong temperature dependence of the coupling coefficient. This indeed can be observed in the above figure. The behaviour of the coupling coefficient directly reflects the temperature dependence of the electron collisions which are involved in the spin changing transition. It is of interest to note how the coupling coefficient decreases as the temperature increases.

We now consider the dependency of the cross coupling coefficient on the nuclear charge of typical impurity species. Once again we emphasise that the electron density is fixed and the number density of impurity ions is such that charge neutrality is maintained. In figure 6.12 we show the behaviour of the coupling coefficient corresponding to the transition He(2 ^{1}S)→He(2 ^{3}S) for a selected range of pure impurity plasmas.

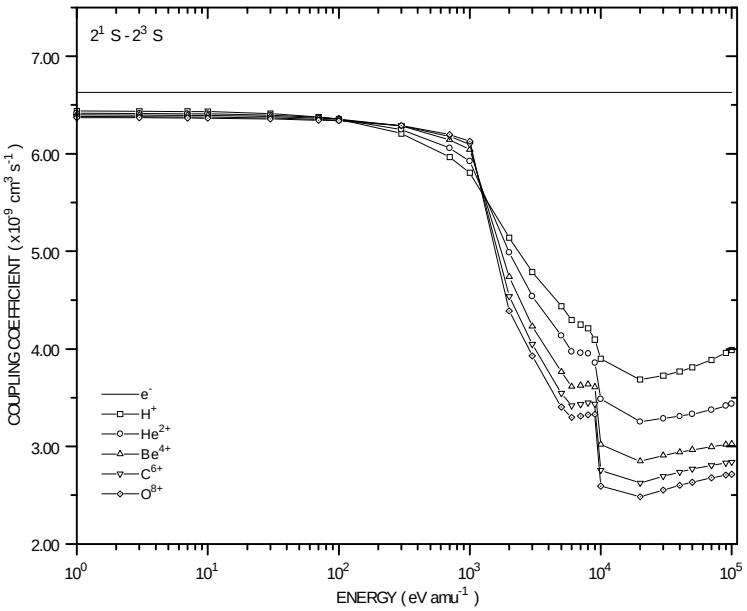

Figure 6.12 Cross coupling coefficient for the transition He(2 ^{1}S)→He(2 ^{3}S) for a selected range of pure impurity plasmas. Also shown is the contribution to the coefficient due to electrons only. The electron density and temperature were respectively 1.0×10^{13} cm^{-3} and 100 eV. The number density of impurity ions is such that charge neutrality is maintained.

The greater the nuclear charge of the impurity species the more effective it is at encouraging collisional redistribution amongst the excited states and opening up additional reaction pathways associated with the He(2 ^{1}S) metastable. Also shown in the figure is the coupling coefficient due to electrons only. It is of interest to note that even at very low beam energies, the contribution to the coupling coefficient due to the some of the impurity ions is of significance. The driving mechanism for the impurity ions in this regime is their thermal ion temperatures.

The parameter dependencies of the remaining cross coupling coefficients contained in the spin changing group show a similar parameter dependency. As an example we show in figure 6.13 the behaviour of the coupling coefficient for the transition He(2 ^{3}S)→He(2 ^{1}S) for a pure D^+ plasma.

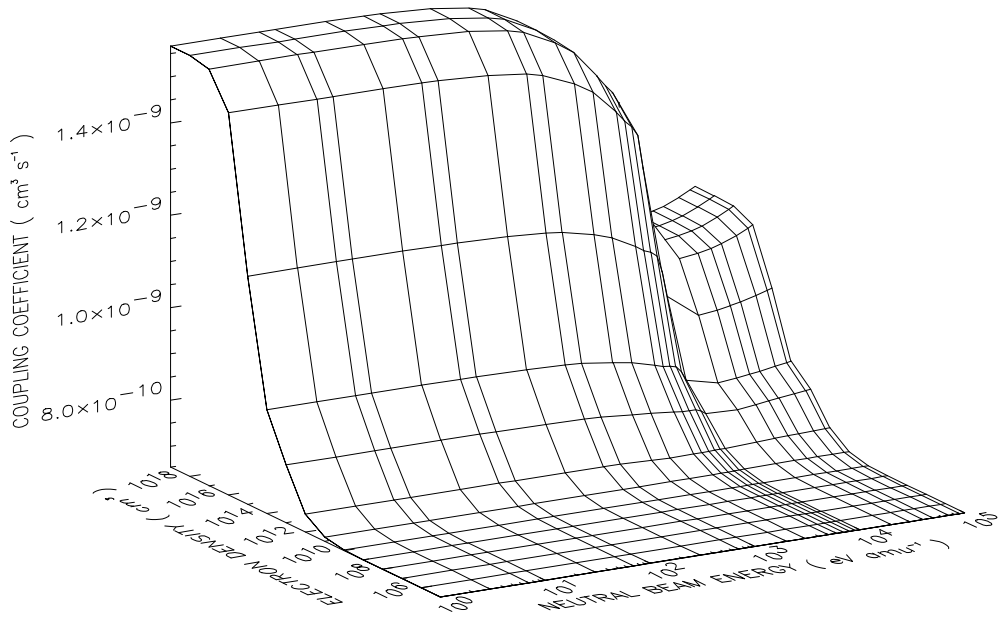

Figure 6.13 Behaviour of the He(2 ^{3}S)→He(2 ^{1}S) cross coupling coefficient for a pure D^+ plasma. In the low density regime the coefficient is independent of the neutral beam energy since it driven purely by electron collisions. As we increase the density the influence of the ion collisions open up additional reaction pathways associated with the He(2 ^{3}S) and a decrease in the coefficient can be observed.

As can be observed, in the low density regime the cross coupling coefficient is independent of the neutral beam energy. As the electron density is increased the role of the ion collisions opens up additional reaction pathways associated with the He(2 ^{3}S) metastable. It is instructive to compare the above figure with the surface plot shown in figure 6.7. In the latter figure, which shows the behaviour of the coupling coefficient describing the loss rate from the He(2 ^{3}S) metastable, we can see that as the electron density and neutral beam energy is increased the influence of the ion collisions result in the electrons being preferentially ionised. This is consistent with the above figure, which shows that as the electron density and beam energy is increased the reaction rate for the transition He(2 ^{3}S)→He(2 ^{1}S) substantially decreases

6.3.3 Collisional-radiative ionisation coefficients

It of interest to show the behaviour of the effective ionisation coefficients associated with the ground state and each metastable. However it is important to note that even though we can assign an effective ionisation coefficient to each non-equilibrium level and hence an effective stopping coefficient in principle, to implement a numerical attenuation calculation involves solving a set of coupled equations which describe how the metastable and ground state populations evolve as the beam traverses the plasma. Due to the presence of metastable levels we can not describe the attenuation of the beam with a single coefficient. The helium beam attenuation calculation, which is the subject of section 6.5, is analogous to modelling the attenuation of three beams which are not independent of each other. In figure 6.14 we show the general behaviour of the effective ionisation coefficients associated with each level for a pure D^+ plasma. The effective ionisation rates associated with the He(2 ^{1}S) and He(2 ^{3}S) metastable levels are order of magnitudes greater than the ionisation coefficient associated with the ground state. A similar behaviour is shown by both ionisation coefficients. In the low density and energy regime each of the coefficients are purely driven by electron collisions. As the neutral beam energy is increased the contribution due to ion collisions results in a sudden increase in the effective coefficients. As we increase the electron density the contribution due to stepwise processes results in a further increase until the high density limit is reached.

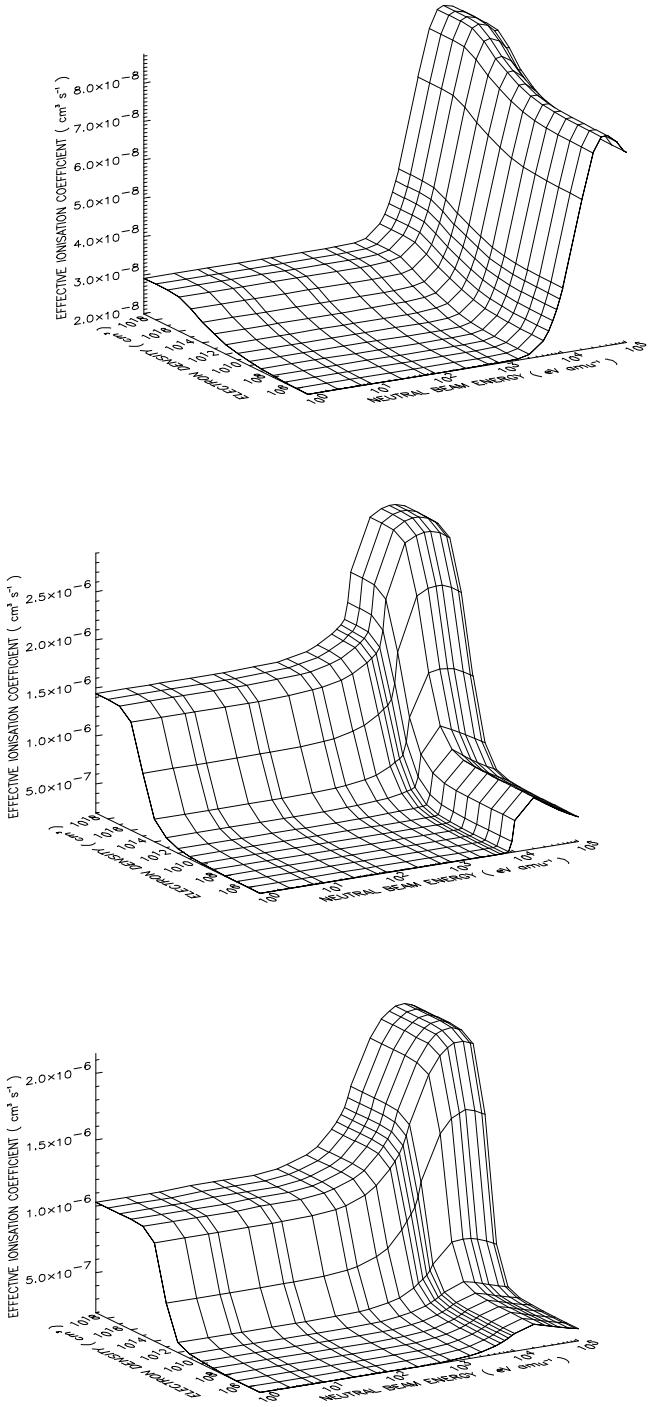

Figure 6.14 Collisional-radiative effective ionisation coefficients for a pure D^+ plasma. Starting from the top we show the effective coefficients associated with the ground state and then the He(2 ^{1}S) and He(2 ^{3}S) metastables. As can be observed the magnitude of the coefficients associated with the two metastable levels are substantially greater than the ionisation coefficient associated with the ground state. The electron temperature was fixed at 100 eV.

6.4 Quasi-static excited state population structure

In this section we illustrate the dependence of the excited population structure on the neutral beam energy, electron density and the electron temperature. We also show the influence of the metastable levels on the excited population structure, particularly the n=4 shell. Since the excited states have reached equilibrium relative to the ground state and the two metastables, it is of interest to be able to identify the extent to which each metastable is responsible for driving the population of each of the excited levels. For the higher levels above the He($3\ ^3D$) this certainly is not obvious. Finally, we illustrate the dependency of the excited population structure on the nuclear charge of the impurity ions. We have restricted our study of the excited levels up to the n=4 shell, since this encompasses the important levels for visible spectroscopy. The quasi-static population of these levels have been calculated in a resolved $nl^{2S+1}L$ picture up to the n=5 shell which then continues into a bundled-nS picture and terminates at n = 110.

6.4.1 Neutral beam energy dependence

The efficiency of the ion collisions in collisional redistribution and ionisation of the excited population structure is beam energy dependent. Also since ion collisions are spin conserving we would expect their influence to be confined within a spin system. In figure 6.15 we show the excited population structure of the singlet and triplet spin systems relative to the He($1\ ^1S$) ground state as a function of neutral beam energy for a D^+ plasma.

Considering the singlet spin system, in the low energy regime the excited states are predominantly populated by electron collisions and are independent of the neutral beam energy. There is an insignificant contribution by ion collisions, due to their thermal temperature. As the beam energy is increased the influence of the ion collisions becomes significant. This results in a decrease in the excited state populations which can be attributed to ion impact ionisation depopulating each of the levels. If we continue to increase the beam energy the depleted populations begin to recover and increase as a function of beam energy. This is due to the fact that it becomes more energetically favourable to populate most of the levels by ion impact

excitation than to depopulate each of them by ion impact ionisation. The extent to which each level is populated depends on their associated ionisation energy and the excitation energy required to populate the level from the nearest neighbour. For example, if we consider the He(3 ^{1}P) level, the ionisation energy is ~1.499 eV while the excitation energy to populate this level from the He(3 ^{1}S) is only ~0.166 eV. We would therefore expect the population of He(3 ^{1}P) level to increase as ion impact excitation strongly competes with ion impact ionisation. However if we consider a higher lying level, for example He(4 ^{1}S), in this case ion impact ionisation will have a larger influence than the contribution due ion impact excitation from neighbouring levels and we would expect the increase in the He(4 ^{1}S) population to be of less significance as shown in figure 6.15.

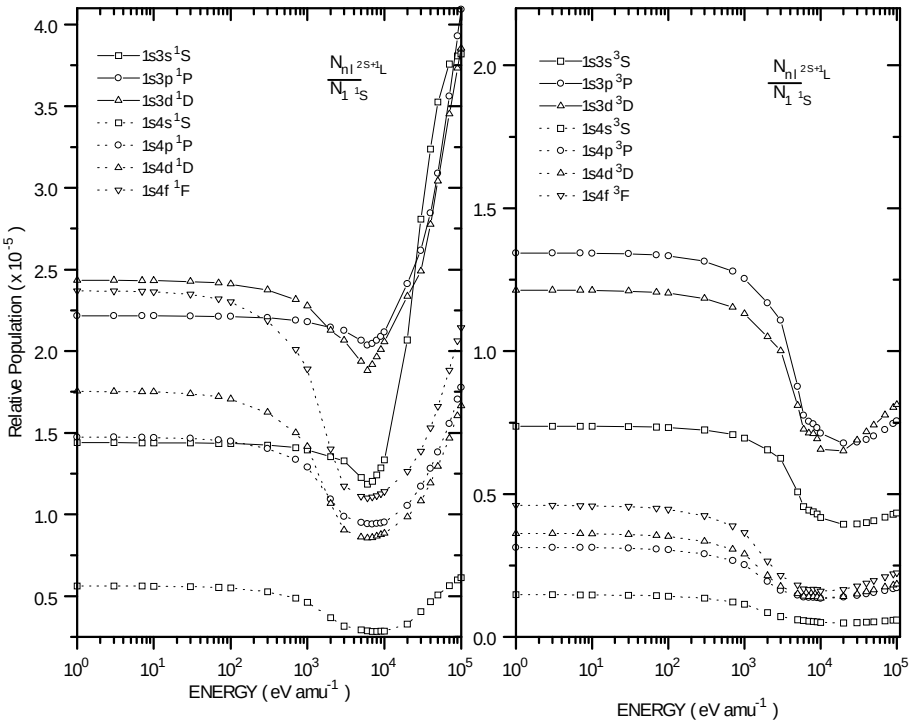

Figure 6.15 Quasi-static excited state populations of the singlet and triplet spin system relative to the He(1 ^{1}S) ground state for a D^+ plasma. The plot to the left shows the population structure of the singlet spin system while the figure to the right illustrate population structure of the triplet spin system. The electron density was 1.0×10^{13} cm^{-3} and the temperature was 100 eV.

If we now consider the population structure of the triplet spin system driven by the He(1 ^{1}S) ground state, as mentioned before, only electron collisions are responsible for populating the triplet spin system. This can occur through direct excitation from the ground state or via spin changing transitions from the excited states of the singlet to the triplet spin system. As shown in figure 6.15, in the low energy regime the population structure is independent of the neutral beam energy. However as we increase the beam energy the excited triplet populations can be observed to decrease. This is due to the fact that as we increase the beam energy, ion impact ionisation which promotes the singlet populations to the continuum becomes important. The singlet populations decrease and the contribution from the excited state spin changing collisions to the triplet spin system is reduced. If we continue to increase the beam energy the population of the triplet levels can be observed to slightly recover. This is due to the rise in the populations of the singlet spin system and hence an increase in the contribution to the population of the triplets due to excited state spin changing transitions.

A similar type of behaviour can be observed for the singlet and triplet populations relative to the He(2 ^{1}S) and He(2 ^{3}S) metastable levels, see figure 6.16. It should be noted though, that in both these cases it is more energetically favourable to populate the excited levels of the singlet spin system via ion impact excitation, than to depopulate them by ion impact ionisation. Therefore the extent to which the excited states of the singlet spin system are depopulated is minimal.

The singlet populations relative to the He(2 ^{1}S) and He(2 ^{3}S) metastables can be observed to decrease slightly as a we increase the beam energy. The populations however soon rapidly recover due to the contribution from ion impact excitation, see figure 6.16.

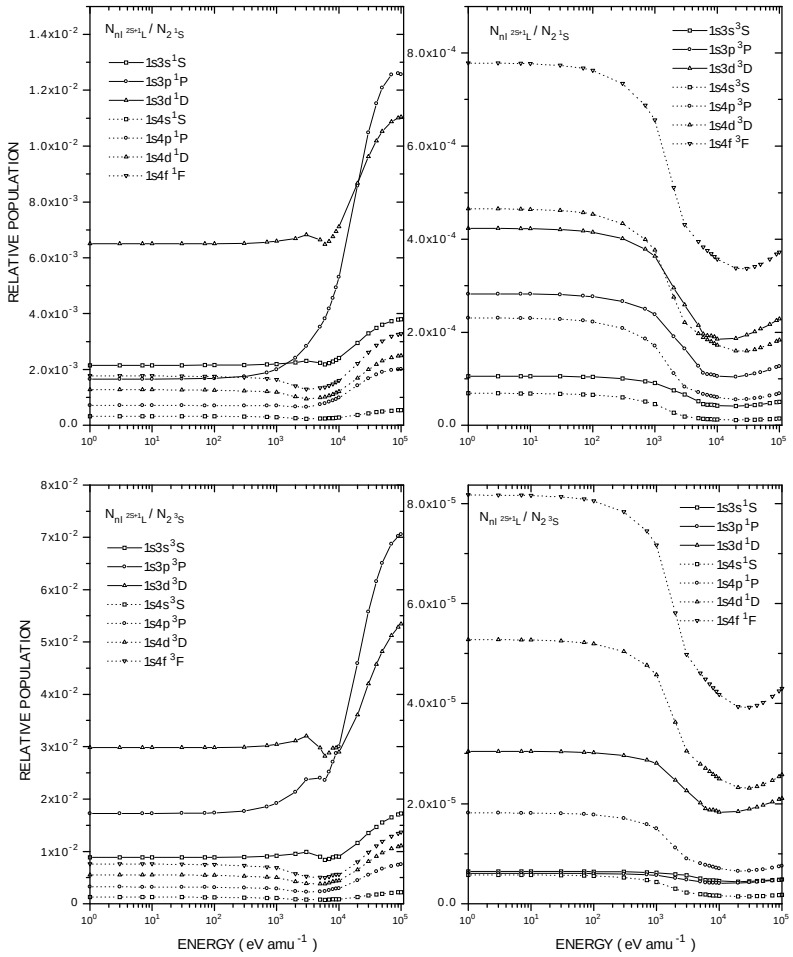

Figure 6.16 Quasi-static excited population structure of the singlet and triplet spin systems relative to the He(2 ^{1}S) and He(2 ^{3}S) metastable levels for a D^+ plasma. The two plots at the top show the behaviour of the singlet and triplet excited population structure relative to the He(2 ^{1}S) metastable. The two plots at the bottom show the behaviour of the excited population structure relative to the He(2 ^{3}S) metastable. The electron density was 1.0×10^{13} cm^{-3} and the temperature was 100 eV.

6.4.2 Density dependence

In figure 6.17 we show the behaviour of the singlet and triplet population structure relative to the He(1 ^{1}S) ground state as a function of electron density for a D^+ plasma.

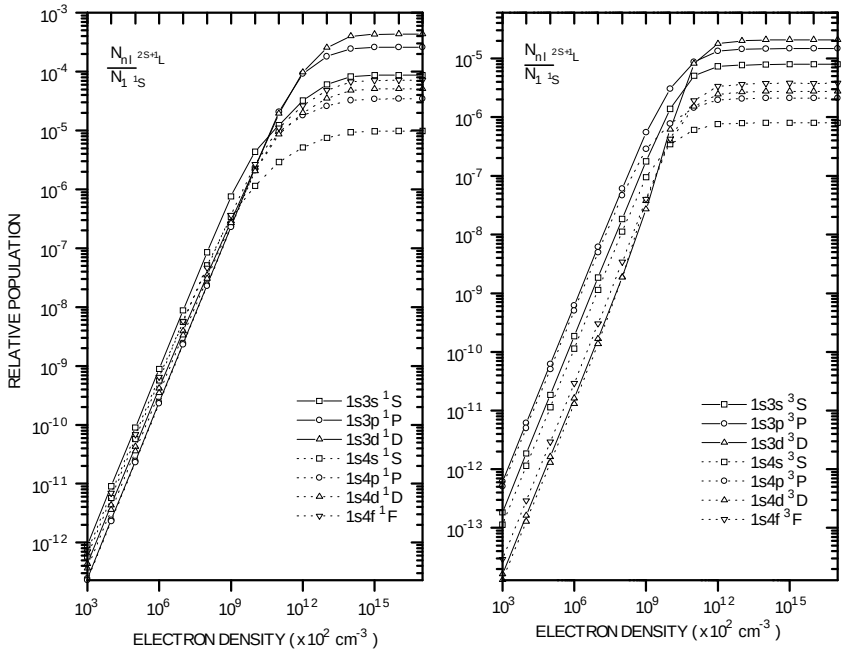

Figure 6.17 Quasi static excited population structure of the singlet and triplet spin system relative to the He(1 ^{1}S) ground state for a D^+ plasma. The beam energy and temperature are respectively 5.0 keV amu^{-1} and 100 eV. The populations are calculated in terms of the electron density but it is in fact the ion collisions which dominate the collisional redistribution. The number density of the ions is such that charge neutrality is maintained.

In the low density regime the excited levels of the singlet spin system associated with the beam atoms are populated by electron and ion collisions. The triplet spin system is populated by electron collisions. Regardless of the spin system the excited levels are depopulated by radiative decay. The excited populations relative to the He(1 ^{1}S) ground state are directly proportional to the electron density. At 1.0×10^{13} cm^{-3} in figure 6.17 we are in the collisional-radiative regime. As we continue to increase the electron density the excited populations reach the high density limit. A similar parameter dependency of the singlet and triplet population structure, relative to the He(2 ^{1}S) and He(2 ^{3}S) metastable levels, is shown in figure 6.18.

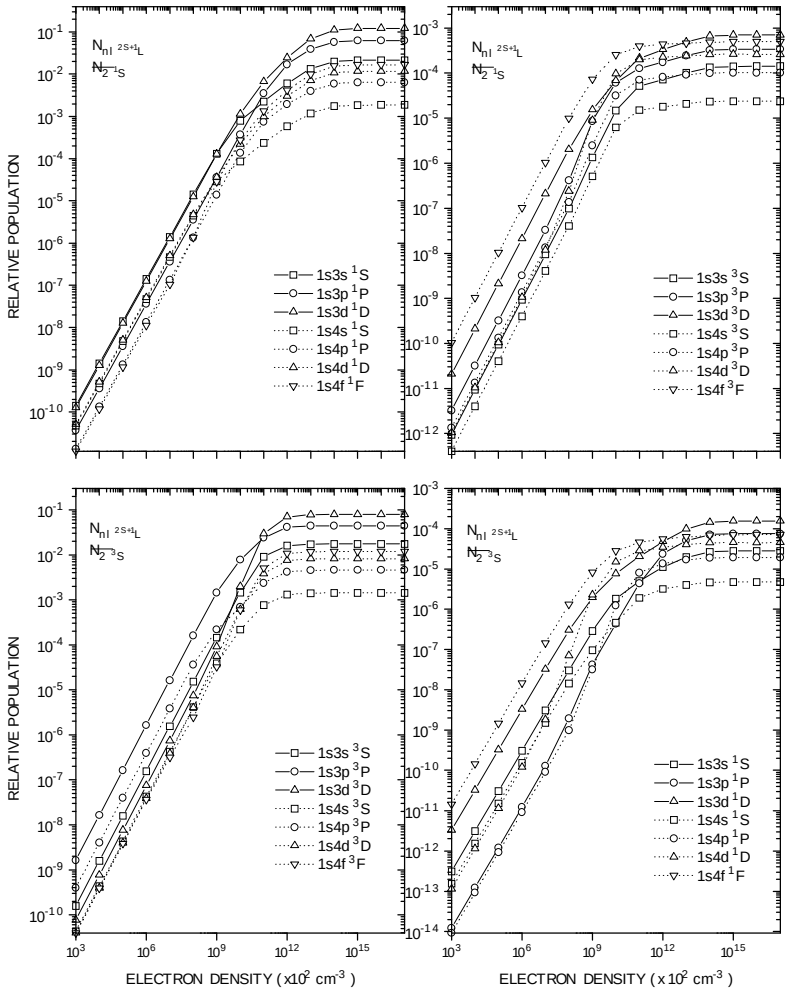

Figure 6.18 Quasi-static equilibrium populations of the singlet and triplet spin systems relative to the He(2 ^{1}S) and He(2 ^{3}S) metastables for a D^+ plasma. The beam energy and temperature are respectively 5.0 keV amu^{-1} and 100 eV.

6.4.3 Temperature dependence

In figure 6.19 we illustrate the temperature dependence of the population structure of the singlet and triplet spin system relative to the He(1 ^{1}S) ground state for a D^+ plasma.

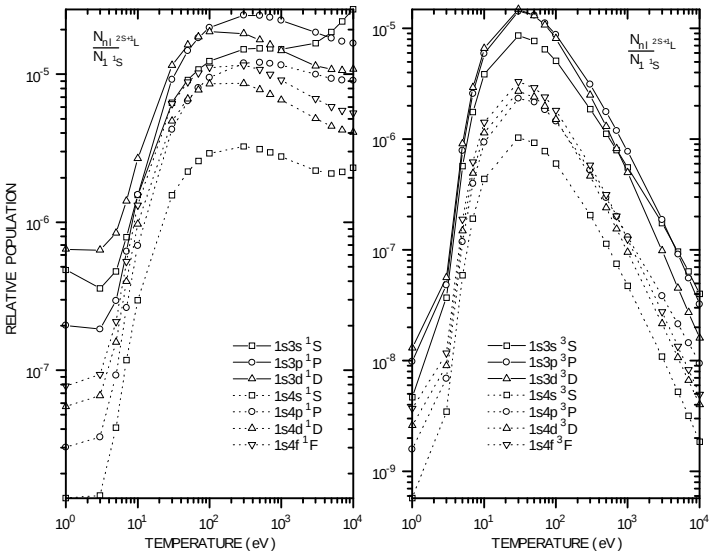

Figure 6.19 Temperature dependence of the quasi-static excited population of the singlet and triplet spin system relative to the He(1 ^{1}S) ground state for a D^+ plasma. The electron density was 1.0×10^{13} cm^{-3} and the neutral beam energy was 5.0 keV amu^{-1}.

As can be observed, the population structure of the triplet spin system is strongly dependent on the electron temperature. This is because the excited states of the triplet spin system can only be populated by electrons collisions via direct spin changing excitation from the ground or via spin changing transitions from the excited states of the singlet spin system. The singlet excited states can be populated by both electrons and ion collisions and the dependency of the electron temperature is some what less. These observations reflect the character of the electron impact excitation rates involved[86]. In terms of the upsilon parameters, these (asymptotic) behaviours are,

Dipole allowed	:	$\gamma_{ij} \sim$ constant . $\ln(T_e)$	6.10
Non Dipole	:	$\gamma_{ij} \sim$ constant	6.11
Spin changing	:	$\gamma_{ij} \sim$ constant. / T_e^2	6.12

For example in the case of the triplet spin system, see figure 6.19, as we increase the electron temperature the rise and decay of the excited state populations directly

reflect the behaviour of the underlying spin changing electron excitation rates. In figure 6.20 we now show the temperature dependence of the singlet and triplet excited population structure relative to the He(2 ^{1}S) and He(2 ^{3}S) metastables, where a similar parameter dependence can be observed.

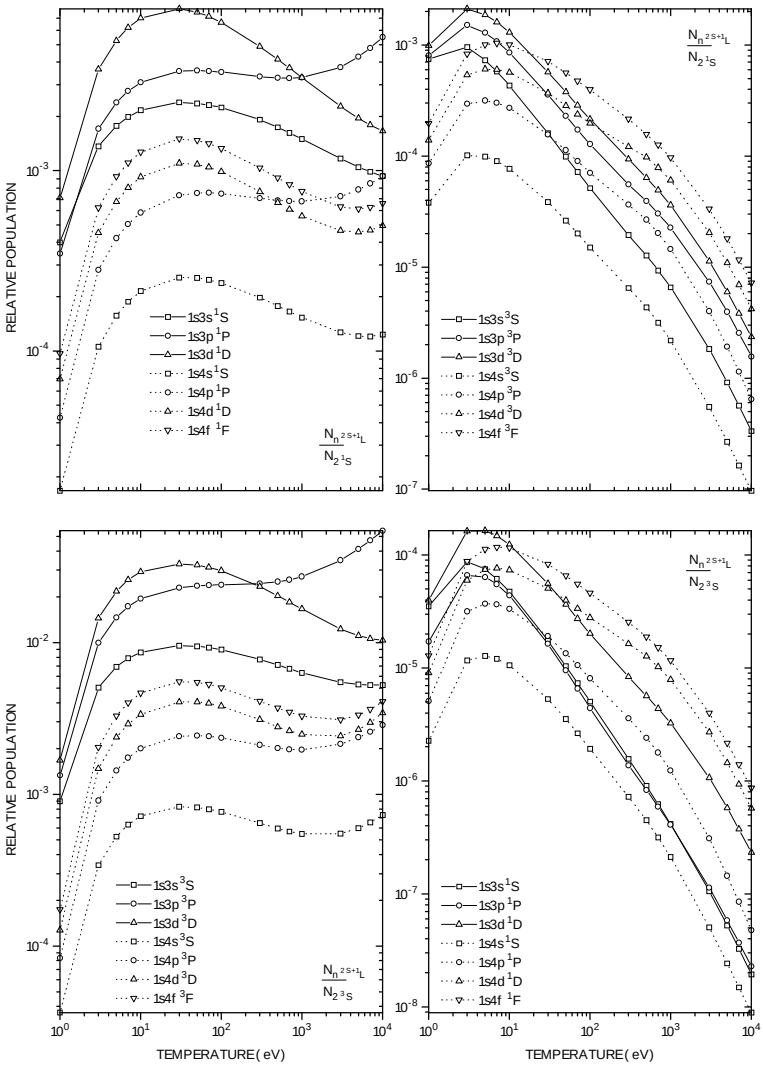

Figure 6.20 Temperature dependence of the quasi-static equilibrium populations of the singlet and triplet spin systems relative to the He(2 ^{1}S) and He(2 ^{3}S) metastable levels for a D^+ plasma. The electron density was 1.0×10^{13} cm^{-3} and the neutral beam energy was 5.0 keV amu^{-1}.

6.4.4 Comparison of the role of the metastable levels

In this sub-section, we summarise the relative importance of the metastables in driving the population structure. We confine our study to the levels contained within the n=4 shell. In figure 6.21 we show the energy dependence of the quasi-static populations of each level contained within the n=4 shell, relative to the ground state and the two metastable levels for a D^+ plasma. By this we mean the contribution functions (FI, FII and FIII) given by equation 3.52. For the singlet spin system it can be seen that the He(2 ^{1}S) metastable is as expected most effective in populating the excited levels within the n=4 shell. It can also be observed that there is a competition between the relative effectiveness of the He(2 ^{3}S) metastable and the He(1 ^{1}S) ground state. If we consider the population of the He(4 ^{1}S) level, we observed that in the low energy regime the contributions from the ground state and the He(2 ^{3}S) metastable are comparable. However as the beam energy increases the contribution from the He(1 ^{1}S) exceeds that from the He(2 ^{3}S) metastable. This is simply due to the fact that the influence of the ion collisions on the singlet spin system is to reduce the He(2 ^{3}S) population's relative importance. If we now study the He(4 ^{1}P) level, in the low energy regime the contribution from the He(2 ^{3}S) metastable is now greater than that from the He(1 ^{1}S) ground state, but as the beam energy increases the effectiveness of the He(2 ^{3}S) metastable decreases and the contribution from the He(1 ^{1}S) dominates. The difference though between the ground state and the triplet metastable, in the high energy regime, is considerably less than that for the He(4 ^{1}S) level. In the case of the He(4 ^{1}D) and He(4 ^{1}F) levels, a similar behaviour in the low energy regime can be observed where the contribution from the He(2 ^{3}S) metastable exceeds that from the He(1 ^{1}S) ground state. However in the high energy regime the contribution from the He(2 ^{3}S) metastable is now greater than that from the ground state. This is quite different from what was observed for the He(4 ^{1}S) and He(4 ^{1}P) levels.

Focusing now on the population structure of the triplet spin system we see that the He(2 ^{3}S) metastable is the dominant non-equilibrium level for populating the excited states contained within the n=4 shell. The contribution from the He(2 ^{1}S)

metastable is considerably less but greater than the contribution from the He(1 ^{1}S) ground state.

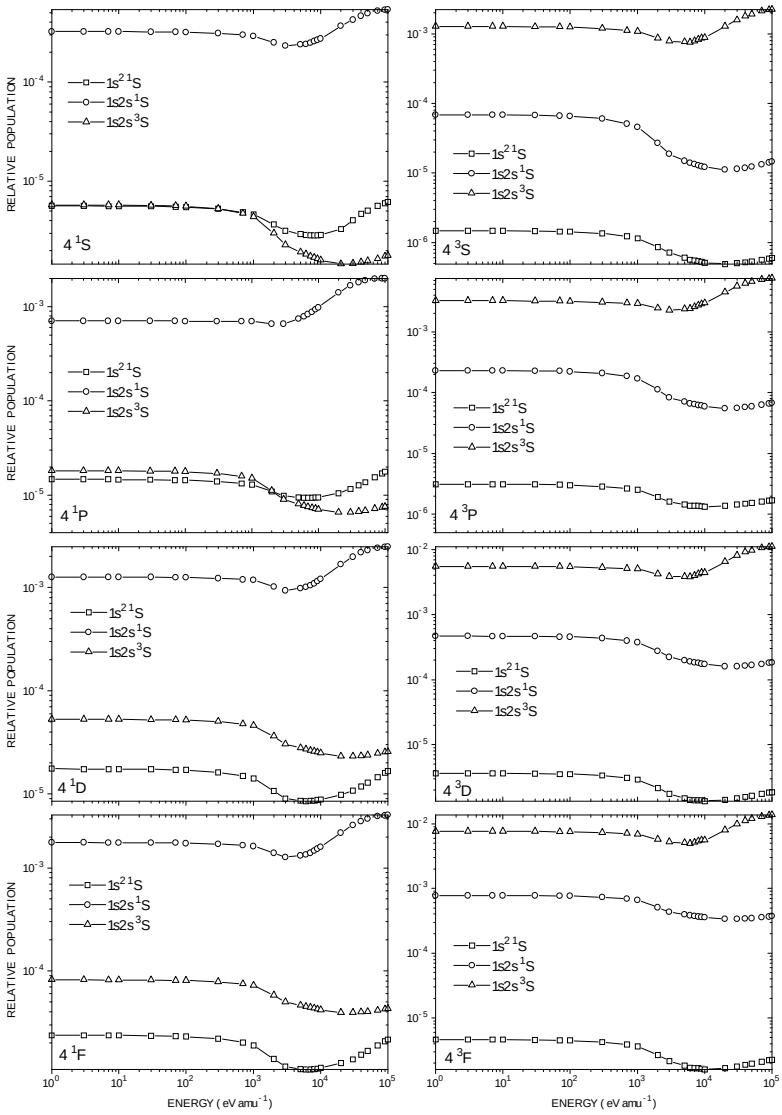

Figure 6.21 Quasi static equilibrium populations of each of the levels contained within the n=4 shell, relative to the ground state and each metastsble level for a D^+ plasma. The plots contained in the column to the left concerns the singlet spin system while column to the right involves the triplet spin system. The electron density was 1.0×10^{13} cm^{-3} and the electron temperature was 100 eV.

In figure 6.22 we now show the density dependence of the quasi-static populations of the levels contained within the n=4 shell, relative to the ground state and the two metastable levels for a pure D^+ plasma.

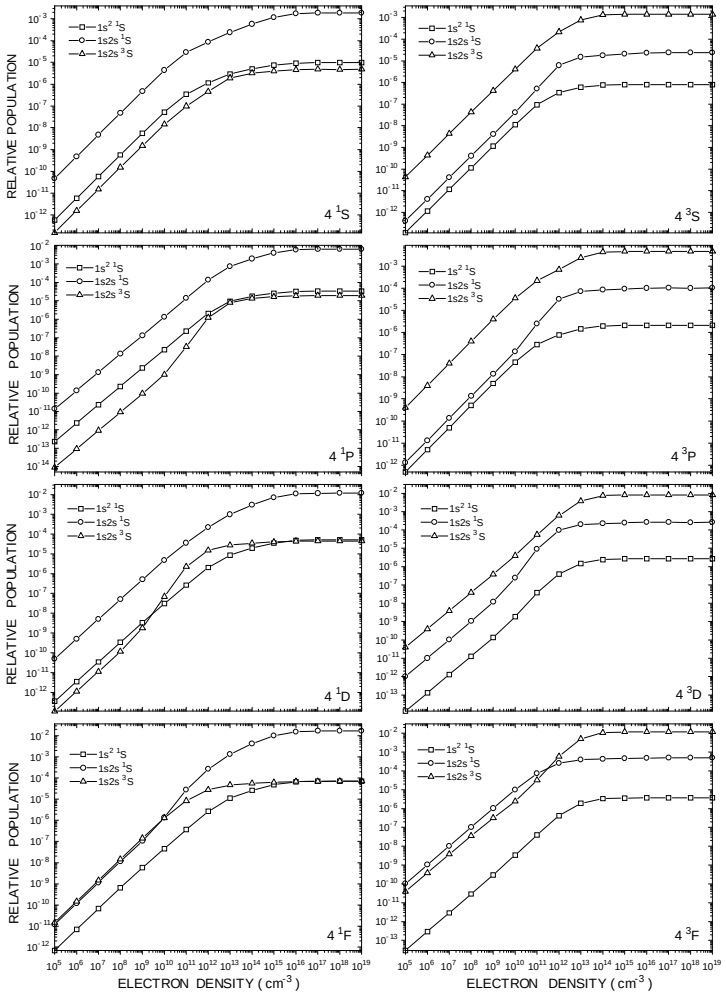

Figure 6.22 Density dependence of the equilibrium populations of the levels contained within the n=4 shell, relative to the ground state and each metastable for a pure D^+ plasma. The electron density was 1.0 x 10^{13} cm^{-3} and the beam energy was 5.0 keV amu^{-1}.

Starting first with the excited populations of the singlet spin system. If we consider the He(4 ^{1}S) level, it can be seen that the contribution from the He(2 ^{1}S) metastable

dominates that from the ground state, which is considerably greater than the contribution from the He(2 ^{3}S) metastable. The He(4 ^{1}P) level exhibits a similar behaviour but we can see the onset of a competition between the contribution from the ground state and the triplet metastable, particular at high densities. This competition is more evident in the case of the He(4 ^{1}D) level where the contribution due to the He(2 ^{3}S) metastable temporarily exceeds that from the ground state. In the case of the He(4 ^{1}F) level we can observe that in the low density region the contribution due to the He(2 ^{3}S) level is even greater than the contribution from the He(2 ^{1}S) metastable. However as the electron density is increased the situation changes.

Similar observation can be made with the populations of the n=4 shell of the triplet spin system. For the He(4 ^{3}S) level the dominant contribution is due to He(2 ^{3}S) metastable and the contribution from the He(2 ^{1}S) level is considerably less but not as small as that from the He(1 ^{1}S) ground state. However as we study the He(4 ^{1}P) level the onset of the competition between the He(1 ^{1}S) and the He(2 ^{1}S) can be observed. This competition continues and for the He(4 ^{1}F), in the low density regime, the contribution from the He(2 ^{1}S) metastable even exceeds that from the He(2 ^{3}S) metastable. As the electron density is increased the He(2 ^{3}S) metastable begins to dominate once again.

We now consider the temperature dependence of the quasi-static population of the levels contained within the n=4 shell, relative to the ground and the two metastable levels for a pure D^+ plasma, see figure 6.23. It can be seen that for the singlet spin system, the dominant non-equilibrium level which is most effective at populating the excited levels is the He(2 ^{1}S) metastable. It can also be observed that there is a competition between the contributions from the He(1 ^{1}S) ground state and the He(2 ^{3}S) metastable level. In the case of all of the excited levels, at relatively low temperatures the contribution due to the He(2 ^{3}S) metastable exceeds that from the He(1 ^{1}S) ground state. However as the temperature increases the opposite occurs and the contribution from the He(1 ^{1}S) ground state is now greater than that from the He(2 ^{3}S) metastable. This type of behaviour is simply due to the temperature dependence of the electron collisions as mentioned earlier.

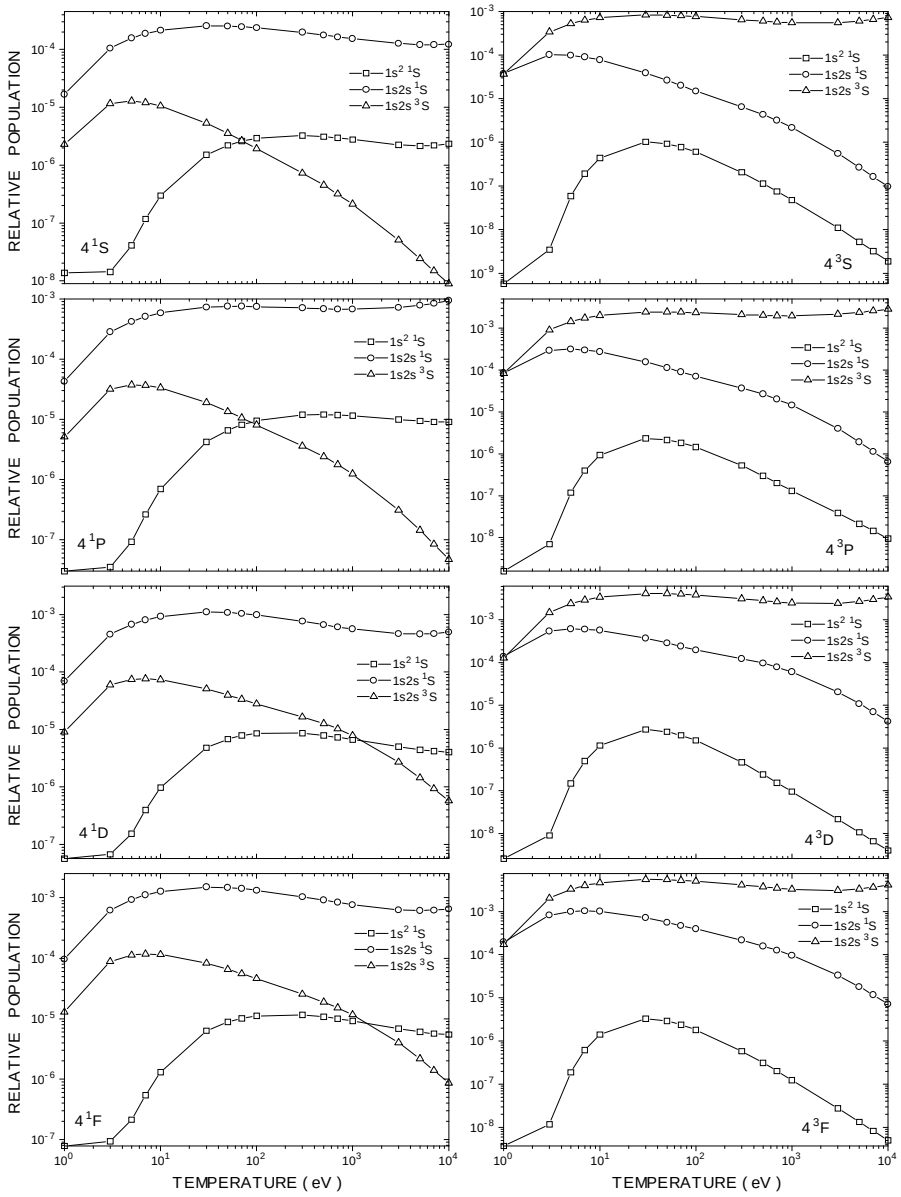

Figure 6.23 Temperature dependence of the quasi static population of the levels contained within the n=4 shell, relative to the ground state and each metastsble level for a pure D^+ plasma. The plots contained in the column on the left concern the singlet spin system while the column on the right pertains to the triplet spin system. The electron density was 1.0 x10^{13} cm^{-3} and the neutral beam energy was 5.0 keV amu^{-1}.

6.4.5 The influence of impurities

Due to the presence of impurities in tokamak plasmas we examine their differential influence on the excited population structure of the beam atoms. We show in figure 6.24 the excited population structure of the singlet spin system relative to the He(1 ^{1}S) ground state for a pure D^+, He^{2+} and C^{6+} plasma.

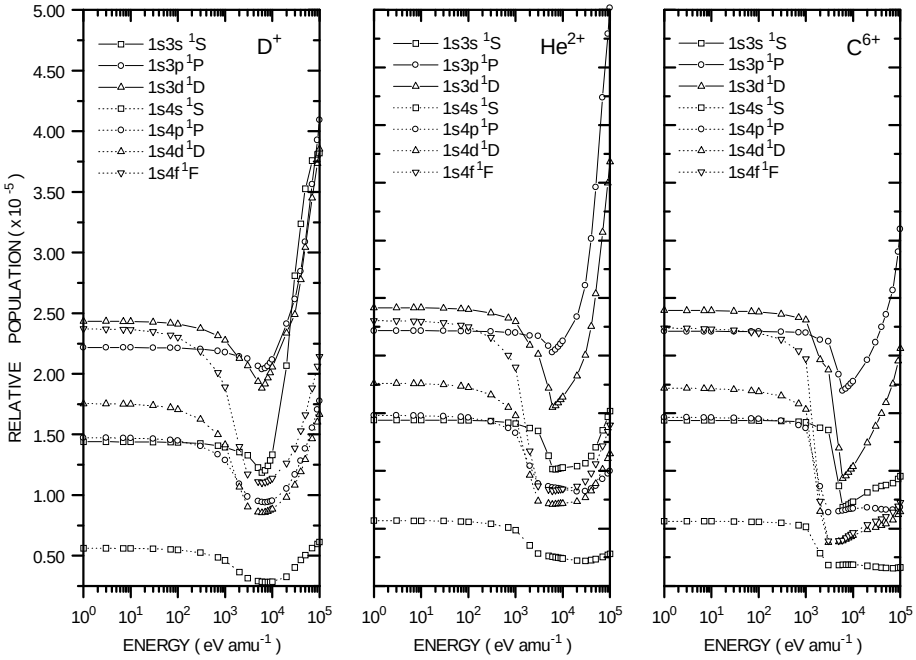

Figure 6.24 Quasi static equilibrium population structure for the singlet spin system relative to the He(1 ^{1}S) ground state. Working from left to right we show the population structure for a pure D^+, He^{2+} and then C^{6+} plasma. The beam energy was 5.0 keV amu^{-1} and the electron density was fixed at 1.0×10^{13} cm^{-3}. The number density of impurity ions is such that charge neutrality is maintained.

If we first confine ourselves to the population structure associated with the beam atoms for a pure D^+ plasma. As mentioned before, we can observe that in low energy regime the population of each level is independent of the beam energy and the contribution due to thermal ion collisions is insignificant. If we now consider the population structure of the beam atoms for a pure He^{2+} plasma. In the low energy regime the small contribution from the ion collisions, due to their thermal velocity, is now larger. As the beam energy is increased the efficiency of the He^{2+} ions at depopulating the excited levels can clearly be observed. We emphasise at this point

that the excited populations are calculated in terms of the electron density, even though it is in fact the ions which are primarily responsible for the collisional redistribution and ionisation of the excited levels. For a fixed electron density the number density of impurity ions is such that charge neutrality is achieved. Therefore with reference to the results shown in figure 6.24, there are twice as many D^+ ions which contribute to modifying the excited population structure than He^{2+} ions. Finally, we consider the population structure of the beam atoms for a pure C^{6+} plasma. The most salient feature which can be seen is the extent to which the excited levels are depopulated due to the influence of ion impact ionisation.

We now consider the excited population structure of the triplet spin system for a pure D^+, He^{2+} and C^{6+} plasma, see figure 6.25.

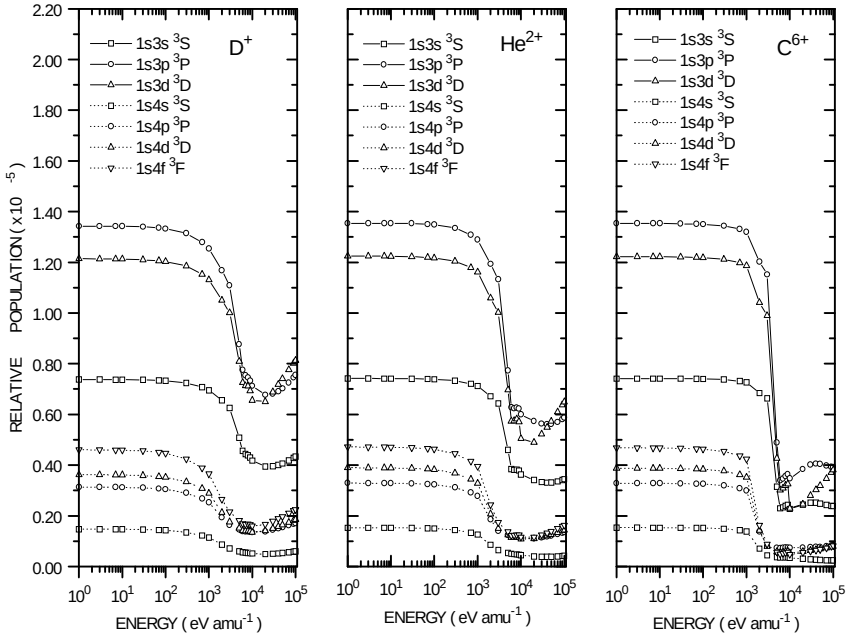

Figure 6.25 Quasi static equilibrium population structure for the triplet spin system relative to the He(1 ^{1}S) ground state. Working from left to right we show the population structure for a pure D^+, He^{2+} and then C^{6+} plasma. The beam energy was 5.0 keV amu^{-1} and the electron density was fixed at 1.0×10^{13} cm^{-3}. The number density of impurity ions is such that charge neutrality is maintained.

In the low energy regime electrons are responsible for populating the excited levels, therefore the excited populations are independent of the neutral beam energy and there is no contribution due to thermal ion collisions. The secondary influence of the

beam energy on the population structure of the triplet spin system can clearly be observed. As the nuclear charge of the plasma impurity ion increases their influence on the triplet spin system is enhanced. In the present work we only considered pure D^+, He^{2+} and C^{6+} plasmas but similar observations can be seen when considering other pure or mixed impurity plasmas.

6.5 Evolution of the metastable populations under JET conditions

If we neglect the metastable nature of the He(2 ^{1}S) and He(2 ^{3}S) levels, then the quasi-equilibrium model would provide the whole population structure including the metastable populations, relative to the ground state. There would be no need to consider the spatial history of each metastable and the attenuation of the beam as a whole would be characterised by only one collisional-radiative coefficient. However in working plasmas the metastables do not reach equilibrium. In this section we calculate the He(2 ^{1}S) and He(2 ^{3}S) metastable populations and contrast with the non-equilibrium metastable populations in an actual beam model. We explore the attenuation of the neutral helium beam and the influence of altering the initial metastable content on entry to the plasma. Finally, we investigate the influence of the electron density and temperature profiles on the beam attenuation.

6.5.1 Method of calculation

We seek the solution of the coupled equations for the metastable and ground state population evolution as the beam traverses the plasma. As discussed earlier we construct the set of such equations using collisional-radiative cross coupling coefficients,

$$\begin{aligned}
v_b \frac{dN_{1^1S}}{dx} &= n_e S_{1^1S} N_{1^1S} - n_e S_{2^1S\to 1^1S} N_{2^1S} - n_e S_{2^3S\to 1^1S} N_{2^3S} \\
v_b \frac{dN_{2^1S}}{dx} &= -n_e S_{1^1S\to 2^1S} N_{1^1S} + n_e S_{2^1S} N_{2^1S} - n_e S_{2^3S\to 2^1S} N_{2^3S} \\
v_b \frac{dN_{2^3S}}{dx} &= -n_e S_{1^1S\to 2^3S} N_{1^1S} - n_e S_{2^1S\to 2^3S} N_{2^1S} + n_e S_{2^3S} N_{2^3S}
\end{aligned} \qquad 6.13$$

We solve for both the metastable and ground state populations relative to the neutral beam density on entry to the plasma. The initial neutral beam density is given by the sum of the ground state and metastable populations. For the quasi-static equilibrium metastable populations the equations reduce to the form,

$$v_b \frac{dN_{1^1S}}{dx} = n_e S_{1^1S} N_{1^1S} - n_e S_{2^1S\to 1^1S} N_{2^1S} - n_e S_{2^3S\to 1^1S} N_{2^3S}$$

$$0 = -n_e S_{1^1S\to 2^1S} N_{1^1S} + n_e S_{2^1S} N_{2^1S} - n_e S_{2^3S\to 2^1S} N_{2^3S} \qquad 6.14$$

$$0 = -n_e S_{1^1S\to 2^3S} N_{1^1S} - n_e S_{2^1S\to 2^3S} N_{2^1S} + n_e S_{2^3S} N_{2^3S}$$

The quasi-static equilibrium population of the He(2 ^{1}S) and He(2 ^{3}S) metastable levels are calculated relative to the He(1 ^{1}S) ground state.

For this work we have written a FORTRAN program which implements the fourth-order Runge-Kutta method to integrate the coupled equations. In addition to solving the equations for the local metastable populations, the program also calculates the corresponding quasi-static equilibrium populations. This enables us to compare the quasi-static populations with the results obtained from our spatially dependent treatment. The program also calculates the attenuation of each metastable including the ground state as a function of radial position. This is useful since it allows one to make an assessment on whether the population of the metastables are significant as the beam continues into the plasma. The main parameters which the program requires as input include the beam energy, the fractional metastable and ground state content of the beam on entry to the plasma, as well as suitable electron density and temperature profiles. A schematic illustration of the program is shown in figure 6.26. The program solves the coupled equations while moving in small increments along a spatial grid, the beginning and end of the grid is defined by the electron density profile. The size of the increments, dx , was selected after running the program several times to obtain a step size which was small enough to ensure numerical convergence but without hugely increasing the computational time of the calculation. In addition to evaluating the coupling coefficients at fixed points along

the grid, the fourth order Runge-Kutta method requires coupling coefficients at intermediate points between the fixed step sizes. The program employs several ADAS library routines to implement the linear interpolation method, see chapter 4.0, to assemble the required coefficients at any point along the working grid.

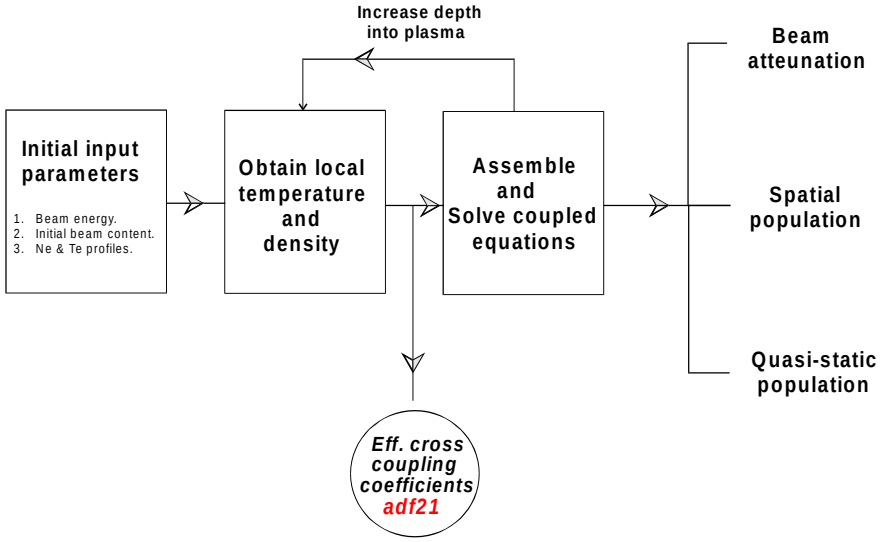

Figure 6.26 Schematic illustration of the FORTRAN program employed to solve the coupled equations which describe the evolution of the ground state and metastable populations. As input the program requires the beam energy, the fractional metastable and ground state content on entry to the plasma, as well as suitable electron density and temperature profiles.

In this study the electron density and temperature profiles, which are used were based on profiles obtained from JET for the pulse number 42676. These can be observed in figure 6.27. Due to the irregular nature of each profile we have fitted 7^{th} order polynomials to each of them using a commercial graph plotting package. This enables us to use the polynomials to look up the electron density and temperature as a function of radial position efficiently. We have also assumed that the plasma for which the model profiles correspond to is of pure deuterium.

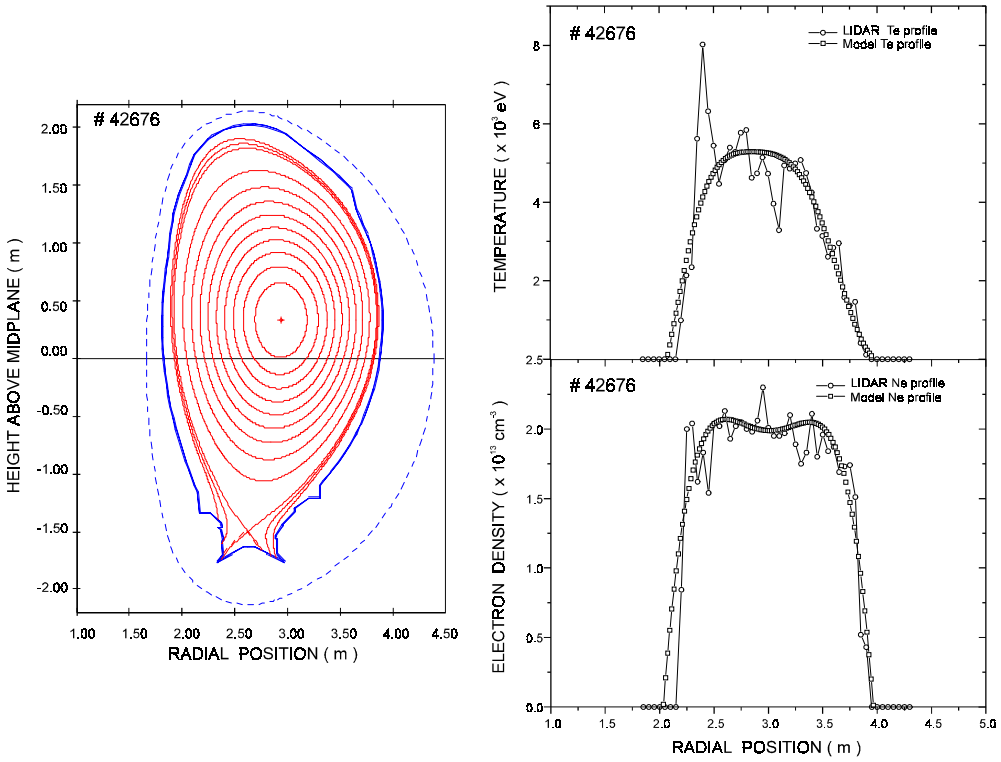

Figure 6.27 Composite figure illustrating the electron density and temperature profiles for the JET pulse 42676. To the left is a schematic of the side elevation of the vessel and should be used as a reference for the radial positions associated with both profiles shown on the right. We have fitted the density and temperature profiles with 7^{th} order polynomials. The motivation for this was to eliminate the irregular structure associated with each profile, also it provided a means of being able to look up the density and temperature as a function of radial position efficiently.

6.5.2 Metastable population : Quasi-static Vs Spatial solution

In working plasmas the scaled lengths (see chapter 2.0) for the electron density and temperature are very short which prevents the metastables reaching equilibrium. In this sub-section we compare the metastable populations from the quasi-static equilibrium model with those of the spatially dependent treatment.

Figure 6.28 shows the population of the He(2 ^{1}S) level relative to the ground state for the case of no metastable content on entry to the plasma.

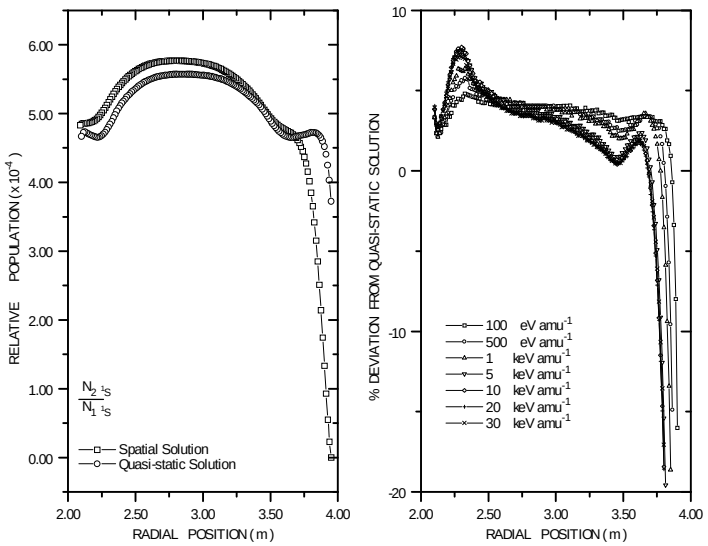

Figure 6.28 Comparison between spatially dependent and quasi-static equilibrium solution for the He(2 ^{1}S) population relative to the ground state. The plot on the left illustrates the behaviour of the quasi-static and spatially dependent He(2 ^{1}S) population for a fixed beam energy of 30 keV amu^{-1}. While the plot on the right shows the percentage deviation of the spatial dependent results from that obtained from the quasi-static assumption for a range of beam energies. On entry to the plasma the total metastable content was zero.

As can be observed there is a significant difference between the results obtained from quasi-static and spatially dependent treatment. This difference is greatest near the edge of the plasma where the scaled lengths for the electron density and temperature are very small, see plot on the left in figure 6.28. If we now consider the results from the core of the plasma around ~ 2.75 m, the difference between the quasi-static picture and the spatial dependent treatment is considerably less. Similar observations can be made from the plot on the right in figure 6.28, where we show the percentage deviation of the spatial dependent results from that obtained from the quasi-static solution for a range of beam energies. Regardless of the beam energy the maximum difference between the quasi-static results and the spatial treatment occurs at the edge of the plasma. In the core of the plasma the He(2 ^{1}S) population does appear to be approaching equilibrium, but does not quite make it within the time scale on which the electron density and temperature change. We can also see from the plot on the left in figure 6.28 the increase in the He(2 ^{1}S) metastable population. Initially the He(2

^{1}S) is zero, however as the beam enters into the plasma, electron and ion impact excitation contributes to populating the He(2 ^{1}S) level.

We show the He(2 ^{3}S) population relative to the ground state. In figure 6.29 the plot to the left shows a comparison between the results obtained from the quasi-static and spatially dependent solution, while the plot on the right shows the percentage deviation of the spatially dependent treatment from that of the quasi-static solution for a range of beam energies.

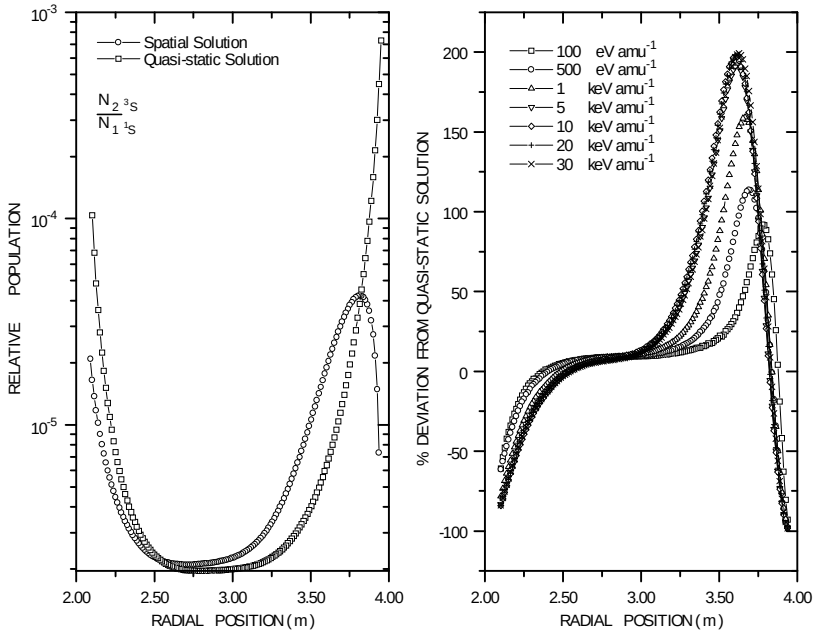

Figure 6.29 Comparison between the quasi-static equilibrium and spatially dependent treatment for the He(2 ^{3}S) population relative to the ground state. The plot to the left illustrates the behaviour of quasi-static and spatial dependent He(2 ^{3}S) population for a fixed beam energy of 30 keV amu^{-1}. The plot to the right shows the percentage deviation of the spatially dependent results from that obtained from the quasi-static assumption. The total metastable content of the beam on entry to the plasma was set to zero.

It can be observed from the spatially dependent solution, shown in the plot on the left in figure 6.29, that as the beam enters the plasma the He(2 ^{3}S) metastable is rapidly populated. This arises due to the fact that the temperature for the first few centimetres into the plasma is optimum (10~200 eV) to promote the influence of spin changing electron collisions, which are the only processes which can populate

the He(2 ^{3}S) metastable level from the ground state. However as the beam continues into the plasma the contribution to the He(2 ^{3}S) level decreases as the electron temperature increases. Above electron temperatures of around ~ 2 keV the contribution due to electron collisions is very small. This prevents the He(2 ^{3}S) metastable population from continuing to increase. As the beam approaches the inner edge of the plasma the spin changing electron collisions become important once again and the He(2 ^{3}S) metastable population increases.

In figure 6.30 we show the quasi-static and spatially dependent populations for the He(2 ^{1}S) and He(2 ^{3}S) metastables, for a beam which initially contains 90 % He(1 ^{1}S) and 10 % He(2 ^{3}S) on entry to the plasma. Practical experiments on neutral helium beam generation indicate that different neutralisation strategies can yield metastable populations of this order.

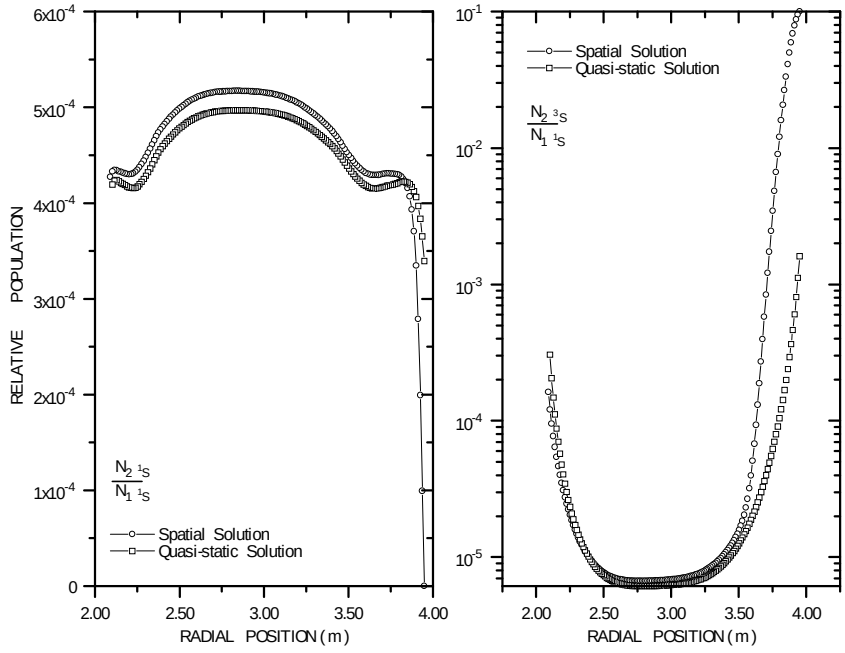

Figure 6.30 Comparison between the quasi-static and spatially dependent populations for the He(2 ^{1}S) and He(2 ^{3}S) metastables. The plot to the left illustrates the behaviour of the quasi-static and spatially dependent He(2 ^{1}S) population. The plot to the right exhibits the behaviour of the quasi-static and spatially dependent population of the He(2 ^{3}S) metastable. On entry to the plasma the contents of the beam consisted of 10% He(2 ^{3}S) and 90 % He(1 ^{1}S).

In the case of the He(2 ^{1}S) metastable, as the beam penetrates into the plasma the He(2 ^{1}S) metastable is suddenly populated and follows the same behaviour as the quasi-static population. The He(2 ^{3}S) metastable population on the other hand is strongly attenuated on entry and as the beam approaches the inner edge of the plasma the He(2 ^{3}S) population can be seen to increase. Finally, in figure 6.31 we consider the hypothetical situation where the contents of the beam on entry to the plasma consists of 90 % He(1 ^{1}S) and 10 % He(2 ^{1}S), even though it would be difficult to prepare a such beam.

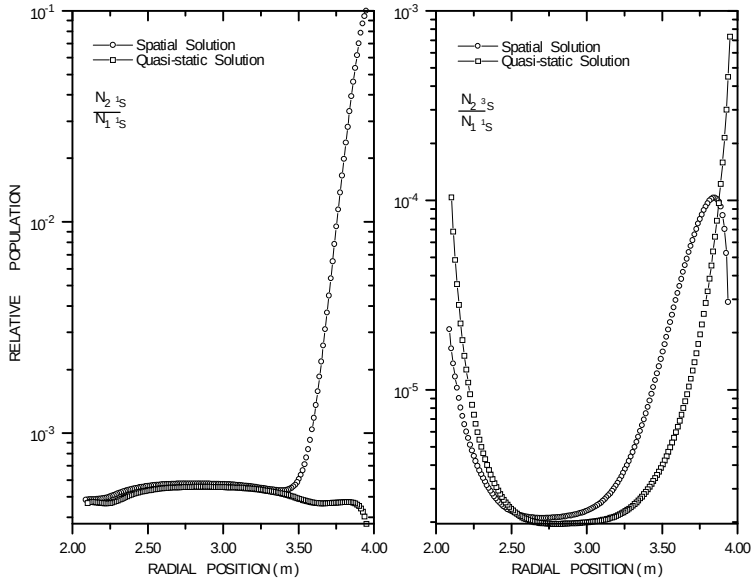

Figure 6.31 Comparison between the quasi-static and spatially dependent populations of the He(2 ^{1}S) and He(2 ^{3}S) metastables. The plot to the left illustrates the behaviour of quasi-static and spatially dependent He(2 ^{1}S) population. The plot to the right exhibits the behaviour of the quasi-static and spatially dependent He(2 ^{3}S) population. On entry to the plasma the beam content consists of 10 % He(2 ^{1}S) and 90 % He(1 ^{1}S).

As can be observed the He(2 ^{1}S) is strongly depopulated as the beam penetrates into the plasma. The He(2 ^{3}S) population exhibits the usual temperature dependence where the population rises at the edge, decrease at the core, and then rises again at the inner edge of the plasma. It is clear that regardless of the initial metastable content in the beam the differences between the metastable populations obtained using the quasi-static approximation and the more accurate spatial dependent treatment is substantial.

6.5.3 Attenuation of a neutral helium beam

In this sub-section we investigate the absolute attenuation of the ground state and metastable levels of a neutral helium beam. We wish to assess if the absolute population of the metastables survive or are regenerated sufficiently for them to act as strong charge exchange donors. This would enable the experimental study of preferential charge exchange donation from the ground state and the metastables levels (c.f. C^{6+} and He^{2+} receivers [85])

The results for zero metastable content on entry into the plasma can be seen in figure 6.32 where we show the attenuation of the He($1\ ^1S$) ground state for a range of beam energies. In the present work, the attenuation of each metastable, including the ground state, is expressed in terms of the corresponding local value relative to the total beam density on entry to the plasma. The total beam density on entry to the plasma is the sum of the ground state and metastable populations.

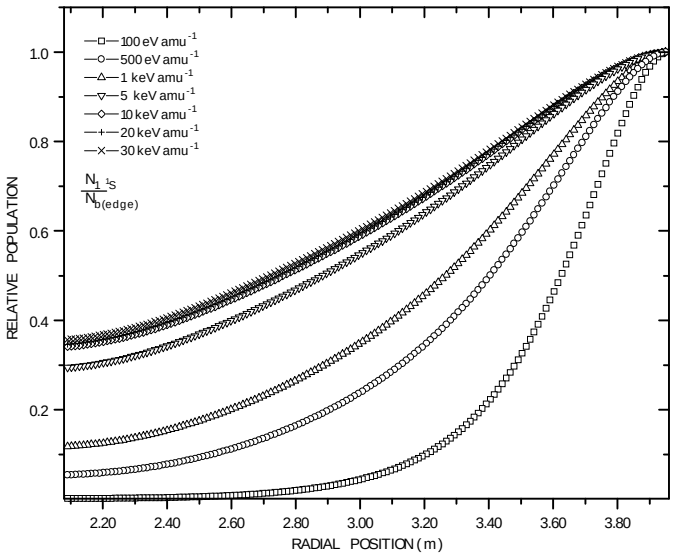

Figure 6.32 Attenuation of the He($1\ ^1S$) ground state for a range of beam energies. The initial metastable content of the beam was set to zero. The electron and temperature profiles used are shown in figure 6.27.

As shown in figure 6.32, for a relatively slow beam it is strongly attenuated at the edge of the plasma. As we increase the beam energy the attenuation of the ground

state population becomes less and for a beam of 30 keV amu^{-1} a total shine through of approximately 36 % is achieved. We show in figure 6.33 the behaviour of the He(2 ^{1}S) and He(2 ^{3}S) populations as a function of radial position relative to the initial beam density on entry to the plasma.

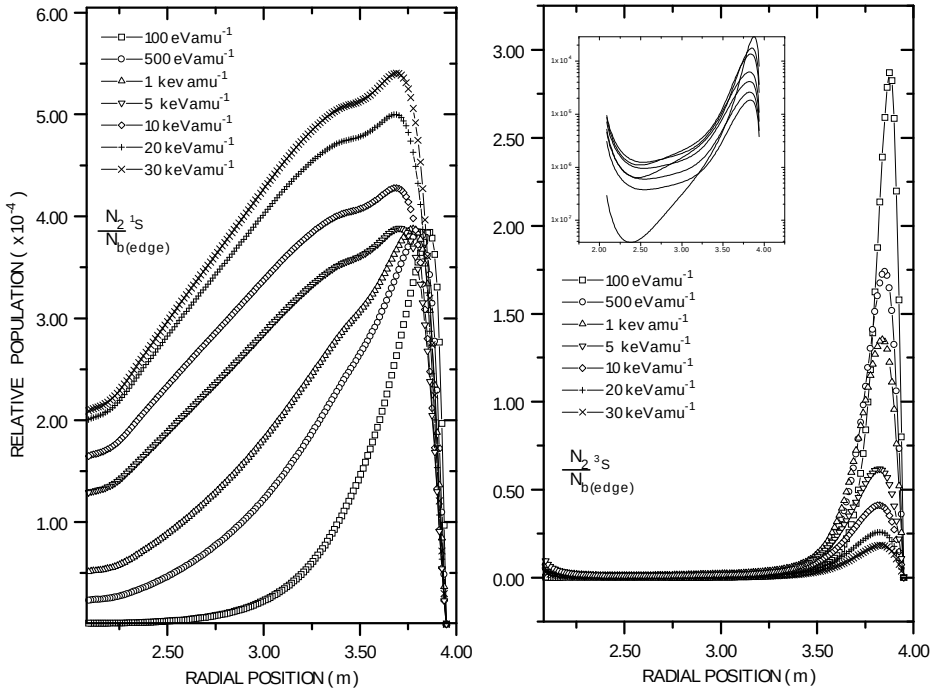

Figure 6.33 Attenuation of the He(2 ^{1}S) and He(2 ^{3}S) metastable levels. The electron density and temperature profiles used are shown in figure 6.27. It is interesting to note that the initial metastable population was zero on entry to the plasma. Therefore it is clear that there is a sudden rise in the both the He(2 ^{1}S) and He(2 ^{3}S) populations at the edge of the plasma.

If we confine ourselves with the behaviour of the He(2 ^{1}S) metastable which can be seen in the plot on the left in figure 6.33, as the beam enters into the plasma the He(2 ^{1}S) level is suddenly populated and then slowly decays as the beam penetrates through the plasma. For a slow beam the He(2 ^{1}S) metastable is attenuated relatively quickly. The behaviour of the He(2 ^{3}S) metastable is shown in the plot to the right in figure 6.33. As with the He(2 ^{1}S) level we can also see a similar increase in the He(2 ^{3}S) level as the beam just enters into the plasma. As the beam continues into the plasma the He(2 ^{3}S) population is attenuated very rapidly. At the inner edge of the

plasma we can observe that the He(2 ^{3}S) population begins to increase again. This is also shown in the insert contained in the plot shown in figure 6.33. The behaviour of the He(2 ^{3}S) metastable directly reflects the strong temperature dependence of the electron collisions, see section 6.4.1.

In figure 6.33 the populations of each metastable are well below 0.1 % of the initial beam density on entry to the plasma. We question whether it is necessary to take into consideration the influence of the metastables while modelling the attenuation of a beam, for which the metastable content on entry to the plasma is zero. We have tabulated in table 6.1, the percentage of the He(1 ^{1}S) population, which is attenuated as a function of penetration depth for a range of beam energies. Also shown in a separate table, table 6.2, is the percentage of the He(1 ^{1}S) population which is attenuated when we now neglect the He(2 ^{1}S) and He(2 ^{3}S) metastables in the attenuation calculation.

Penetration Depth (m)	Neutral beam energy (keV amu^{-1})						
	0.1	0.5	1.0	5.0	10.0	20.0	30.0
0.25	36.47	18.88	14.24	8.44	7.46	7.20	7.43
0.50	72.93	45.23	35.72	22.37	19.96	19.24	19.79
0.75	89.90	.65.15	53.88	35.81	32.27	31.16	31.94
1.00	96.24	77.93	67.01	47.02	42.78	41.42	42.36
1.25	98.63	86.12	76.53	56.51	51.80	50.28	51.31
1.50	99.52	91.49	83.61	64.51	59.76	58.16	59.24
1.75	99.78	94.08	87.44	69.52	64.81	63.21	64.31

Table 6.1 Helium beam attenuation for which the initial metastable content was set to zero. The tables contain the percentage of the beam which is attenuated as function of penetration depth for a range of beam energies.

Penetration Depth (m)	Neutral beam energy (keV amu^{-1})						
	0.1	0.5	1.0	5.0	10.0	20.0	30.0
0.25	36.46	18.86	14.21	8.40	7.43	7.11	7.31
0.50	72.93	45.23	35.71	22.35	19.94	19.19	19.72
0.75	89.90	65.16	53.87	35.79	32.26	31.17	31.97
1.00	96.24	77.94	67.01	47.01	42.78	41.47	42.44
1.25	98.70	86.46	76.94	56.84	52.22	50.77	51.86
1.50	99.52	91.51	83.61	64.51	59.77	58.27	59.40
1.75	99.78	94.09	87.45	69.53	64.82	63.30	64.43

Table 6.2 Helium beam attenuation for which the initial metastable content was set to zero. The tables contain the percentage of the beam which is attenuated as function of penetration depth for a range of beam energies. In this case the metastable nature of He(2 ^{1}S) and He(2 ^{3}S) has been ignored in the attenuation calculation.

The influence of the metastable levels while modelling the beam attenuation is negligible. Therefore if interest is only in determining the total beam density as a function of penetration depth, for a beam in which the initial metastable content on entry to the plasma is zero, we can neglect the metastable levels. The attenuation of the beam can be characterised using a single collisional-radiative ionisation coefficient which describes the loss rate from the ground state. It should be emphasised though that to exploit the beam fully as a diagnostic probe via charge exchange spectroscopy, the detailed knowledge of the metastable populations is still required as the associated charge exchange cross sections are very large.

We now investigate the implications of modifying the metastable content of the beam on entry to the plasma. Figure 6.34 shows the attenuation of the He(1 ^{1}S) population for a beam for which the initial contents consists of 90 % He(1 ^{1}S) and 10 % He(2 ^{3}S).

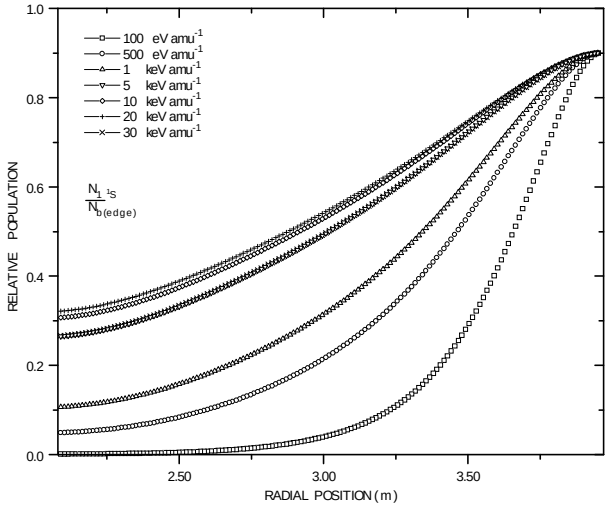

Figure 6.34 Attenuation of the He(1 ^{1}S) population. The initial beam content consists of 90 % He(1 ^{1}S) and 10% He(2 ^{3}S). The electron density and temperature profiles used are shown in figure 6.27.

The attenuation of the He(1 ^{1}S) population, as illustrated in figure 6.34, exhibits the same features as shown for the attention of the He(1 ^{1}S) ground state for a beam for which the initial metastable content was zero, see figure 6.32. In figure 6.35 we show the attenuation of the He(2 ^{1}S) and He(2 ^{3}S) metastable levels for the same conditions. The He(2 ^{1}S) population exhibits the same features which we highlighted

earlier, namely a sudden increase in the metastable level marking the entry of the beam and then the population decay. The He(2 ^{3}S) metastable enters the plasma with a 10 % population, therefore we do not see the sudden rise in the population due to contribution from electron collisions. As the beam penetrates into the plasma we can see the population being strongly attenuated and then near the inner edge of the plasma, the He(2 ^{3}S) population begins to rise again, see inset contained in the plot on the right in figure 6.35. Due to the large ionisation coefficient associated with the triplet metastable the attenuation is substantial. For example, the He(2 ^{3}S) population for a beam energy of 100 eV amu^{-1} is attenuated by ~ 55 % within approximately 6 cm of entering the plasma.

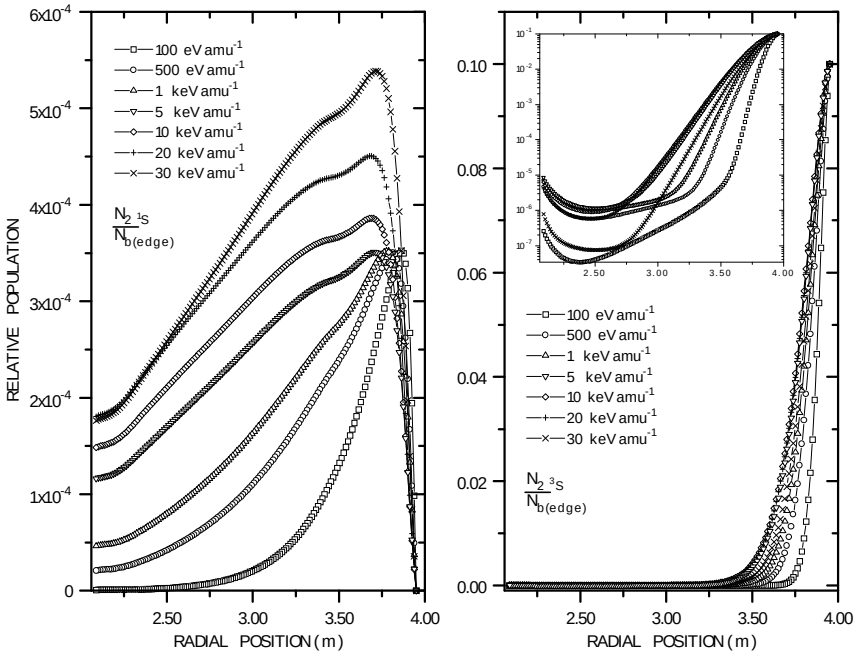

Figure 6.35 Attenuation of the He(2 ^{1}S) and He(2 ^{3}S) metastable levels. On entry to the plasma the beam content consisted of 10 % He(2 ^{3}S) and 90 % He(1 ^{1}S). The electron density and temperature profiles used are shown in figure 6.27.

In table 6.3 we have tabulated the percentage of the He(2 ^{3}S) metastable population which is attenuated as a function of the penetration depth for a range of beam energies. We have also shown two additional tables (tables 6.4 & 6.5) which illustrate the attenuation of the He(2 ^{3}S) metastable as the initial metastable population is increased.

90 % He(1 ^{1}S) 10 % He(2 ^{3}S)

Penetration Depth (m)	Neutral beam energy (eV amu^{-1})						
	100	500	1000	5000	10,000	20,000	30,000
0.0124	6.10	2.90	2.20	1.40	1.30	1.30	1.70
0.0248	14.60	7.20	5.40	3.60	3.40	3.50	4.40
0.0372	24.70	12.50	9.50	6.50	6.20	6.30	8.00
0.0496	35.30	18.60	14.30	9.90	9.50	9.70	12.40
0.0620	45.80	25.20	19.60	13.80	13.20	13.60	17.20

Table 6.3 Attenuation of the He(2 ^{3}S) metastable as a function of penetration depth for a range of beam energies. The tables contain the percentage of the beam which is attenuated as function of penetration depth for a range of beam energies. The initial beam content was 90 % He(1 ^{1}S) and 10 % He(2 ^{3}S).

80 % He(1 ^{1}S) 20 % He(2 ^{3}S)

Penetration Depth (m)	Neutral beam energy (eV amu^{-1})						
	100	500	1000	5000	10,000	20,000	30,000
0.0124	6.12	2.92	2.18	1.42	1.33	1.33	1.41
0.0248	14.70	7.21	5.45	3.63	3.43	3.47	3.69
0.0372	24.77	12.57	9.58	6.52	6.20	6.31	6.72
0.0496	35.42	18.68	14.38	9.96	9.51	9.72	10.35
0.0620	45.92	25.27	19.66	13.84	13.25	13.56	14.44

Table 6.4 Attenuation of the He(2 ^{3}S) metastable as a function of penetration depth for a range of beam energies. . The tables contain the percentage of the beam which is attenuated as function of penetration depth for a range of beam energies. The initial beam content was of 80 % He(1 ^{1}S) and 20 % He(2 ^{3}S).

70 % He(1 ^{1}S) 30 % He(2 ^{3}S)

Penetration Depth (m)	Neutral beam energy (eV amu^{-1})						
	100	500	1000	5000	10,000	20,000	30,000
0.0124	6.13	2.92	2.19	1.42	1.33	1.33	1.41
0.0248	14.73	7.22	5.46	3.64	3.43	3.48	3.69
0.0372	24.80	12.59	9.59	6.53	6.20	6.31	6.72
0.0496	35.46	18.70	14.40	9.97	9.51	9.72	10.36
0.0620	45.97	25.29	19.68	13.84	13.26	13.56	14.44

Table 6.5 Attenuation of the He(2 ^{3}S) metastable as a function of penetration depth for a range of beam energies. The tables contain the percentage of the beam which is attenuated as function of penetration depth for a range of beam energies. The initial beam content was 70 % He(1 ^{1}S) and 30 % He(2 ^{3}S).

In figure 6.36 we show the attenuation of the He(1 ^{1}S) ground state for a beam with an initial content comprising of 90 % He(1 ^{1}S) and 10 % He(2 ^{1}S). It can be seen that the He(1 ^{1}S) level shows the usual characteristics. However in figure 6.36, we

observe that the He(1 ^{1}S) population, within a few centimetres of entering the plasma, exceeds its initial value of 90 % due to the rapid transfer from the He(2 ^{1}S) metastable via the He(2 ^{1}P). As we increase the beam energy the net contribution from the He(2 ^{1}S) metastable to the He(2 ^{1}P) level is reduced. This is due to the influence of ion impact ionisation which depopulates the He(2 ^{1}S) metastable.

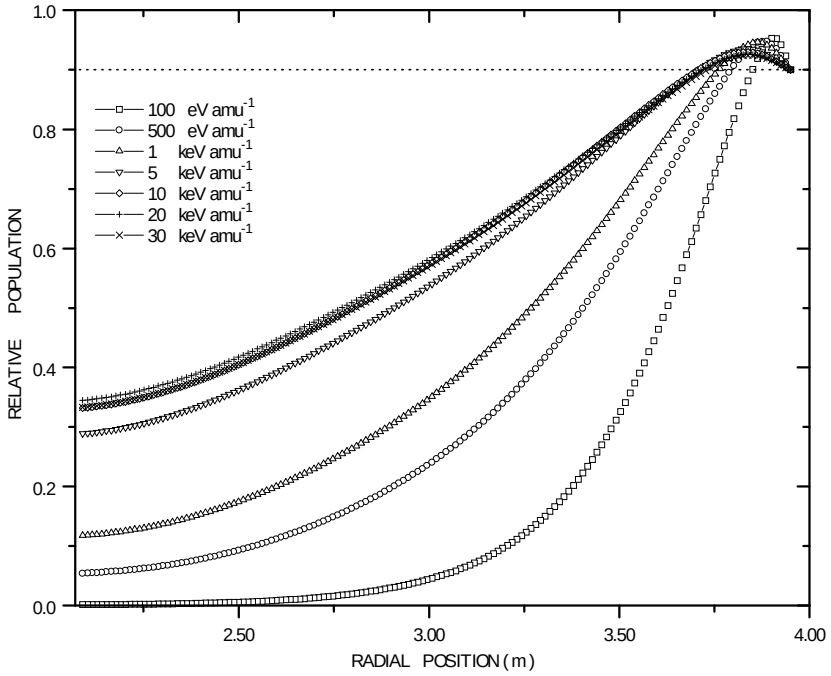

Figure 6.36 Attenuation of the He(1 ^{1}S) ground state as a function of radial position for a range of beam energies. The electron and temperature profiles used are that shown in figure 6.27. On entry to the plasma the beam consisted of 10 % He(2 ^{1}S) and 90 % He(1 ^{1}S).

If we were to increase the initial He(2 ^{1}S) metastable population, the contribution to the ground state population would increase. This can be observed in figure 6.37 where we show the behaviour of the He(1 ^{1}S) population as a function of radial position for different initial He(2 ^{1}S) metastable populations.

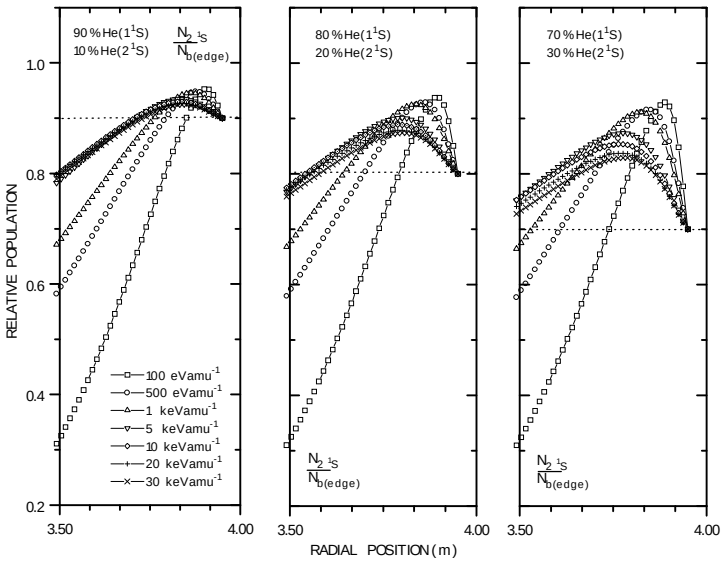

Figure 6.37 Attenuation of the He(1 ^{1}S) ground state as a function of radial position for a range of beam energies. From left to right we show the extent of increase the He(2 ^{1}S) metastable fraction by 10, 20 and 30 %. The electron and temperature profiles used are that shown in figure 6.27.

In figure 6.38 we now show the attenuation of the He(2 ^{1}S) and He(2 ^{3}S) metastables

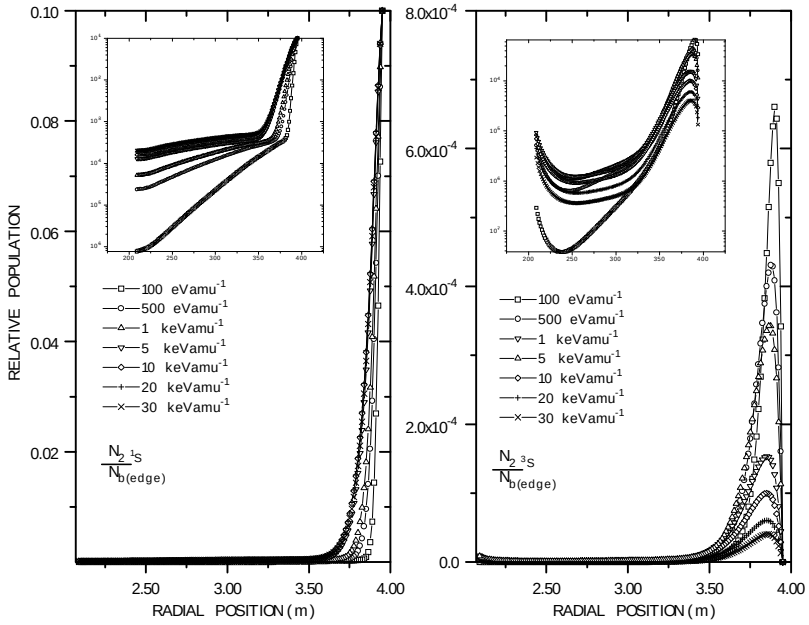

Figure 6.38 Attenuation of the He(2 ^{1}S) and He(2 ^{3}S) metastable as a function of radial position for a range of beam energies. The initial contents of the beam consisted of 10 % He(2 ^{1}S) and 90 % He(1 ^{1}S). The electron density and temperature profiles which were used are shown in figure 6.27.

As can be observed, the He(2 ^{1}S) is also strongly attenuated as the beam enters the plasma. The He(2 ^{3}S) level once again shows the unique rise in population on entry to the plasma and then a decay and then an increase once again. The attenuation of the He(2 ^{1}S) level is strong and merely reflects the large ionisation coefficient associated with the He(2 ^{1}S) level. In table 6.6, we have tabulated the percentage of the He(2 ^{1}S) population which is attenuated as a function of radial position. We have also included two additional tables (tables 6.7 & 6.6) which show similar information but with the initial He(2 ^{1}S) population increased

90 % He(1 ^{1}S) 10 % He(2 ^{1}S)

Penetration	Neutral beam energy (eV amu^{-1})						
Depth (m)	100	500	1000	5000	10,000	20,000	30,000
0.0124	27.30	13.80	10.20	6.40	5.90	5.80	6.00
0.0248	53.50	30.00	22.80	14.70	13.60	13.40	14.00
0.0372	73.10	45.70	35.90	23.90	22.10	21.90	22.90
0.0496	85.50	59.60	48.20	33.30	31.00	30.70	32.00
0.0620	92.67	70.80	59.10	42.30	39.60	39.40	40.90

Table 6.6 Attenuation of the He(2 ^{1}S) metastable level as a function of radial position for a range of beam energies. The tables contain the percentage of the beam which is attenuated as function of penetration depth for a range of beam energies. The initial beam content was 10% He(2 ^{1}S) and 90% He(1 ^{1}S).

80 % He(1 ^{1}S) 20 % He(2 ^{1}S)

Penetration	Neutral beam energy (eV amu^{-1})						
Depth (m)	100	500	1000	5000	10,000	20,000	30,000
0.0124	27.38	13.82	10.24	6.42	5.89	5.79	6.04
0.0248	53.60	30.09	22.84	14.72	13.57	13.41	14.01
0.0372	73.20	45.83	35.94	23.93	22.16	21.96	22.92
0.0496	85.70	59.65	48.50	33.32	31.02	30.81	32.09
0.0620	92.85	70.95	59.25	42.41	39.68	39.46	41.00

Table 6.7 Attenuation of the He(2 ^{1}S) metastable level as a function of radial position for a range of beam energies. The tables contain the percentage of the beam which is attenuated as function of penetration depth for a range of beam energies. The initial beam content was 20 % He(2 ^{1}S) and 80 % He(1 ^{1}S).

70 % He(1 ^{1}S) 30 % He(2 ^{1}S)

Penetration Depth (m)	Neutral beam energy (eV amu^{-1})						
	100	500	1000	5000	10,000	20,000	30,000
0.0124	27.40	13.83	10.25	6.42	5.90	5.79	6.04
0.0248	53.61	30.04	22.86	14.73	13.58	13.42	14.02
0.0372	73.23	45.85	35.96	23.95	22.18	21.98	22.94
0.0496	85.76	59.70	48.33	33.35	31.04	30.83	32.12
0.0620	92.90	70.96	59.30	42.44	39.71	39.49	41.04

Table 6.8 Attenuation of the He(2 ^{1}S) metastable level as a function of radial position for a range of beam energies. The tables contain the percentage of the beam which is attenuated as function of penetration depth for a range of beam energies. The initial beam content was 30 % He(2 ^{1}S) and 70 % He(1 ^{1}S).

On comparing the results contained in table 6.3 and 6.6, the former of which concerns the attenuation of the He(2 ^{3}S) metastable, we can see that under the present plasma conditions the He(2 ^{1}S) metastable is attenuated at a greater rate.

Finally, we consider the scenario where both of the metastable levels are populated on entry to the plasma. We show in figure 6.39 the behaviour of both the He(2 ^{1}S) and He(2 ^{3}S) levels as a function of radial position. The initial content of the beam comprises of 5 % He(2 ^{1}S), 5 % He(2 ^{3}S) and 90 % He(1 ^{1}S).

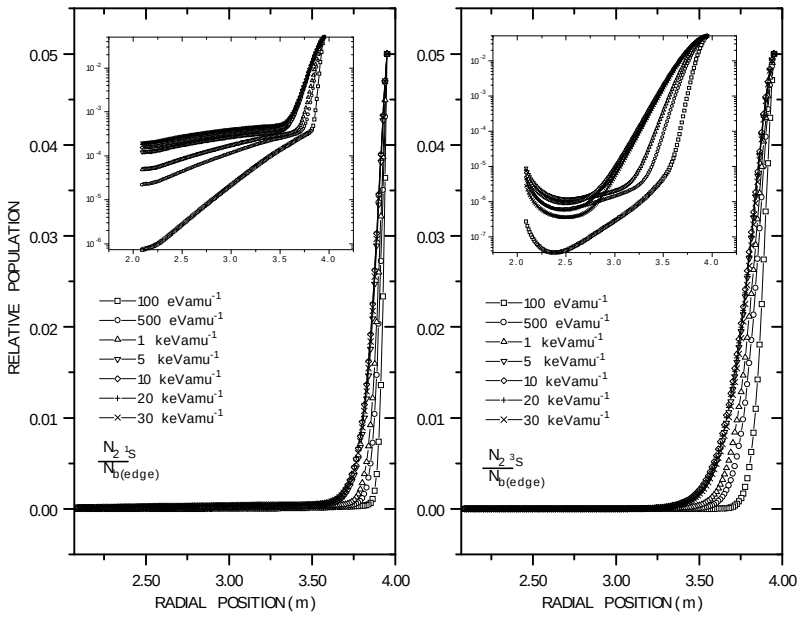

Figure 6.39 Attenuation of the He(2 ^{1}S) and He(2 ^{3}S) metastable levels . The initial content of the beam consisted of 5 % He(2 ^{1}S), 5 % He(2 ^{3}S) and 90 % He(1 ^{1}S). The electron density and temperature profiles can be seen in figure 6.27.

From figure 6.39 we can see that the He(2 ^{1}S) metastable is attenuated faster than the He(2 ^{3}S) metastable. Both metastables show the typical behaviour as a function of radial position which has been described before.

6.5.4 Additional physics of helium beam attenuation

In tokamak plasma such as JET, fluctuations in the electron temperature and density are common, e.g. see figure 3.27. In this sub-section we explore the influence of such rapid changes on the attenuation of the ground state and the metastable levels. However rather than contrast the beam attenuation using profiles from different types of plasma, we have opted to use theoretical profiles. These profiles have been selected specifically to illustrate the influence due to sudden changes. In our study we only consider the attenuation of a helium beam, for which the initial metastable content on entry to the plasma is zero.

6.5.4.1 Influence of the electron temperature profile

The electron temperature profile which we have selected is sinusoidal in nature and oscillates between a value of 10 eV to 6 keV as a function of radial position. The electron density profile which is employed is as before and can be seen in figure 6.40 together with the hypothetical electron temperature profile.

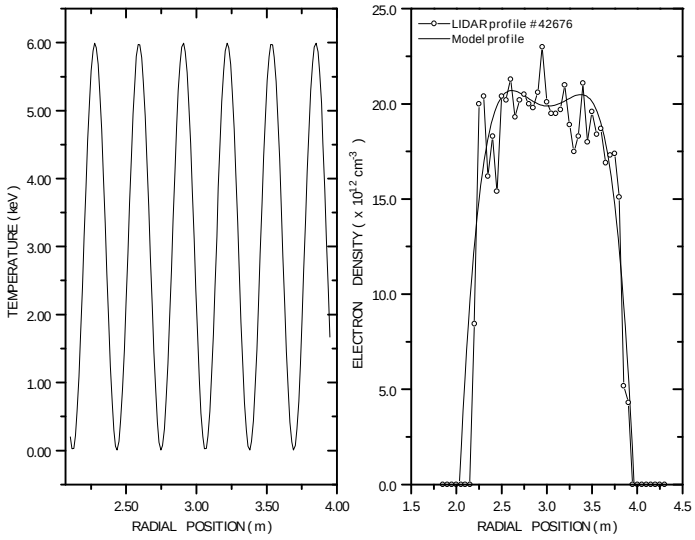

Figure 6.40 Electron temperature and density profile. The temperature profile oscillates between 10 eV and 6 keV. The electron density profile was obtained from the JET pulse 42676, to remove the irregular features we have fitted the profile with a smooth curve.

In figure 3.41 we show the attenuation of He(2 ^{1}S) and He(2 ^{3}S) metastable populations as a function of radial position. The influence of the temperature profile on the He(1 ^{1}S) was negligible.

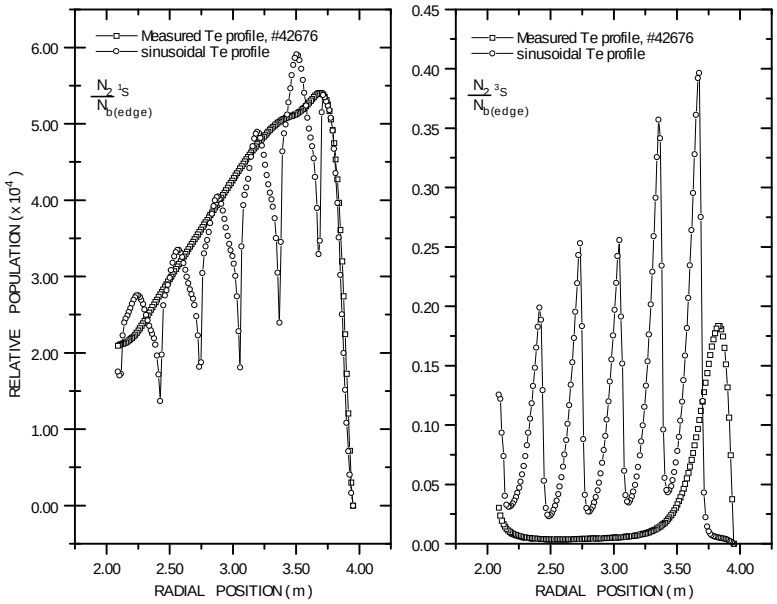

Figure 6.41 Influence of the electron temperature profile on the attenuation of the He(2 ^{1}S) and He(2 ^{3}S) metastable populations. The electron density which was used is that shown in figure 6.40. The initial metastable content of the beam was zero. Also shown is the attenuation of each of the metastable populations using the temperature profile as shown in figure 6.27. The beam energy was 30 keV amu^{-1}.

The attenuation of each metastable has a rather curious temperature dependence. In the case of the He(2 ^{1}S) metastable, as the beam enters the plasma the metastable is rapidly populated. The populating mechanism is primarily due to ion collisions since the edge temperature is greater than 1.5 keV and therefore the contribution due to electron collisions will be small. As the He(2 ^{1}S) population is attenuated it can be observed to show periodic oscillations. The peaks and troughs of these oscillations correspond to when the temperature respectively rises to 6 keV and then falls to 10 eV. When the temperature approaches 10 eV the He(2 ^{1}S) tends to a minimum. The temperature is optimum for spin changing electron collisions which contribute to populating the triplet spin system from the He(2 ^{1}S) metastable. When the

temperature increases the influence of the spin changing electron collisions decreases and the rate at which the He(2 ^{1}S) metastable is depopulated is reduced.

If we now consider the behaviour of the He(2 ^{3}S) population, we can see from figure 6.41 that since the edge temperature is very high, the He(2 ^{3}S) level is scarcely populated on the immediate entry of the beam into the plasma. As the temperature profile approaches a minimum the spin changing cross sections are active and the He(2 ^{3}S) population begins to increase. However as the temperature begins to rise the contribution to the He(2 ^{3}S) metastable is reduced and the population is then strongly attenuated. If we compare the oscillating nature of the He(2 ^{1}S) and He(2 ^{3}S) it can be seen that they are out of phase and when the He(2 ^{1}S) population decreases the He(2 ^{3}S) population suddenly increases as they are both progressively attenuated.

6.5.4.2 Influence of the electron density profile

The electron density profile selected is also sinusoidal in nature and oscillates between 10^{12} to 1.9×10^{13} cm^{-3} as a function of radial position. We show in figure 6.42 both the electron temperature and density profile which are of concern. The electron density profile which is employed is that as described in figure 6.27.

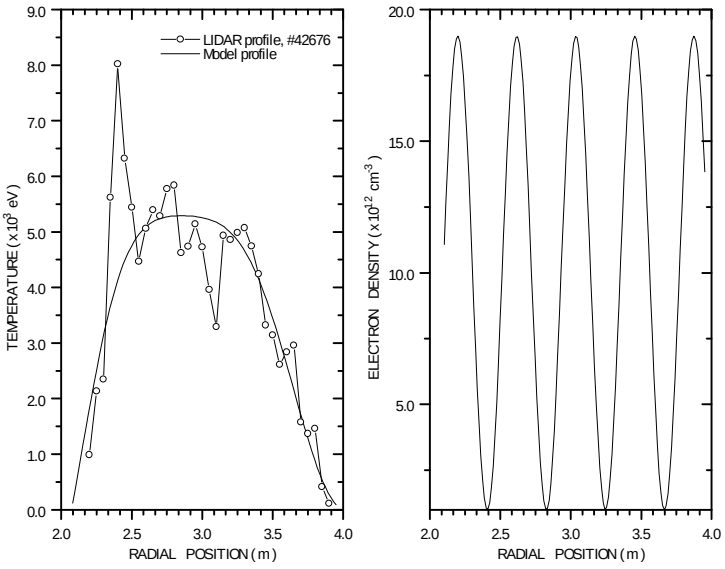

Figure 6.42 Electron density and temperature profiles. The temperature profile was obtained from the JET pulse 42676. The electron density profile oscillates from 10^{12} cm^{-3} to 1.9×10^{13} cm^{-3}.

The behaviour of the He(1 ^{1}S) population as it is attenuated as a function of radial position is shown in figure 6.43. We also show the attenuation of the He(1 ^{1}S) population using the measured electron density profile obtained from the JET pulse 42676.

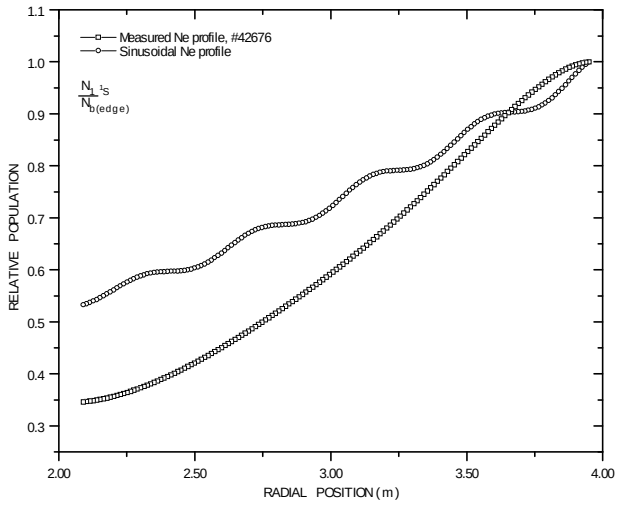

Figure 6.43 Attenuation of the He(1 ^{1}S) for a beam energy of 30 keV amu^{-1}, also shown in the figure is the attenuation of the He(1 ^{1}S) using the model electron density profile obtained from the JET pulses 42676.

It can be seen that as the beam enters the plasma it is immediately attenuated as a result of the high edge plasma density. As the beam continues into the plasma the behaviour of the He(1 ^{1}S) population directly reflects the changes in the electron density profile. When the density profile reaches a minimum the He(1 ^{1}S) remains constant as there is little attenuation. However as the density increases the population of the He(1 ^{1}S) ground state decreases as a results of enhanced attenuation. A similar behaviour can be observed in figure 6.44 where we show the attenuation of the He(2 ^{1}S) and He(2 ^{3}S) metastables.

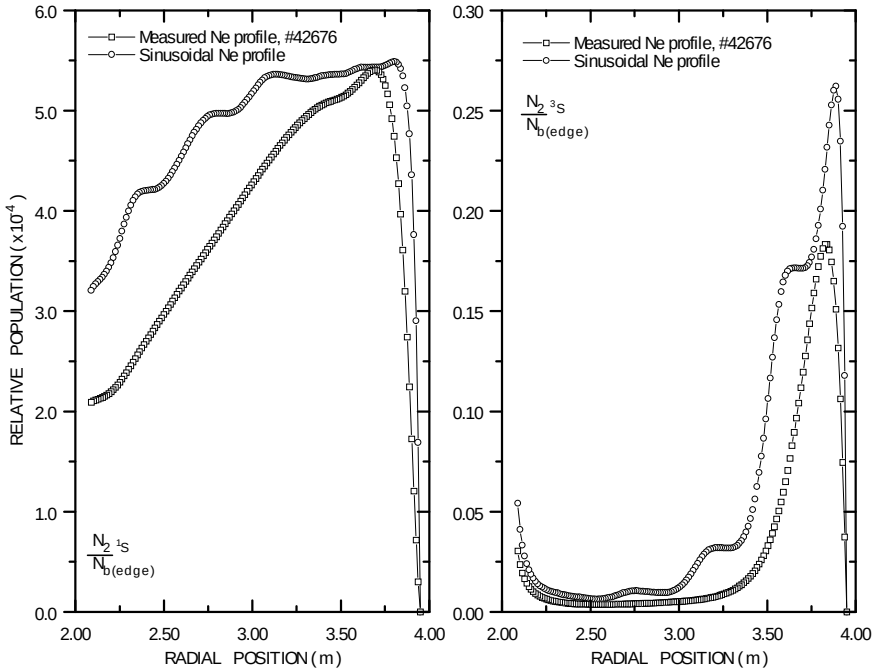

Figure 6.44 Attenuation of the He(2 ^{1}S) and He(2 ^{3}S) for a beam energy of 30 keV amu^{-1}. The initial metastable content of the beam was zero. Also shown in the figure is the attenuation of each metastable using the measured electron density profile obtained from the JET pulses 42676.

6.6 Conclusion

In summary, we have illustrated the behaviour and parameter dependencies of the collisional-radiative cross coupling coefficients. The neutral beam energy determines the efficiency at which the ion collisions contribute to the coupling coefficients. The electron temperature regulates the effectiveness of the electron collisions. The electron collisions contribute to the spin and non-spin changing coupling coefficients. The spin changing coupling coefficients are dominated by electron collisions and are therefore strongly temperature dependent. Ion collisions can only participate in spin conserving collision. We have however identified a secondary dependence of the spin changing coupling coefficients on the beam energy.

The coupling coefficients can be used to define an effective ionisation coefficient associated with the ground state and the metastable levels. These coefficients represent the rate at which each level is ionised and includes the influence of stepwise atomic processes. We have shown that the effective ionisation

coefficients associated with each metastable is substantially greater than the coefficient associated with the ground state. This indicates that once the metastables are populated they will be ionised very quickly in comparison with the ground state.

The Quasi-static excited population structure has been shown to exhibit a similar parameter dependencies to that of the cross coupling coefficients. Electron and ion collisions contribute to populating the singlet spin system while the triplet spin system is only populated by spin changing electron collisions from the ground state. We also considered the influence of impurities on the excited state population structure and examined the extent to which each metastable contributes to populating each of the excited states contained in the n=4 shell.

We have calculated the quasi-static and spatially dependent local metastable population for JET plasma conditions. We have shown that errors can be made by assuming that the metastables have relaxed and reached equilibrium. The extent of which is governed by the beam energy and to a lesser degree the initial metastable content of the beam on entry to the plasma. The beam energy governs the distance the beam atoms can travel within the atomic lifetime of the metastables. If this distance is greater than the scaled lengths associated with the plasma density and temperature, then the metastables will not reach equilibrium. If on the other hand the distance is shorter than the scaled lengths of the plasma dynamics, the metastable levels will relax and reach quasi-static equilibrium.

We have illustrated that the attenuation of a neutral helium beam can be accurately modelled without considering the influence of the metastable populations, provided that the initial metastable population is zero. However consideration of the metastable levels is required if one wants to exploit the possibility of preferential charge exchange from the ground state and the He(2 ^{3}S) metastable. Also for use with beam emission spectroscopy a detailed knowledge of the excited state population structure, including the influence of the metastables, is required.

We have shown that the metastable populations are formed at the edge of the plasma and then rapidly decay as the beam continues into the plasma. For the He(2 ^{3}S) metastable it was shown that the population increases once again as the beam approaches the inner edge of the plasma. The extent of the attenuation of the

metastables is governed by the rate at which they are ionised. We investigated the influence of modifying the initial metastable population of the beam and also the effects due to rapid changes in the electron density and temperature in the plasma.

The influence of the temperature and density profiles is substantial. The temperature had little effect on the attenuation of the He($1\ ^1S$) population while there is an interesting dependency on the He($2\ ^1S$) and He($2\ ^3S$) metastables. The influence of the electron density was more substantive with the He($1\ ^1S$) ground state and the He($2\ ^1S$) metastable level. In summary, the metastable populations are difficult to sustain as the beam traverses the plasma. Nevertheless depending on the initial metastable content, the metastable populations may be of significance for charge exchange and of course spectroscopy.